



저작자표시-비영리-변경금지 2.0 대한민국

이용자는 아래의 조건을 따르는 경우에 한하여 자유롭게

- 이 저작물을 복제, 배포, 전송, 전시, 공연 및 방송할 수 있습니다.

다음과 같은 조건을 따라야 합니다:



저작자표시. 귀하는 원저작자를 표시하여야 합니다.



비영리. 귀하는 이 저작물을 영리 목적으로 이용할 수 없습니다.



변경금지. 귀하는 이 저작물을 개작, 변형 또는 가공할 수 없습니다.

- 귀하는, 이 저작물의 재이용이나 배포의 경우, 이 저작물에 적용된 이용허락조건을 명확하게 나타내어야 합니다.
- 저작권자로부터 별도의 허가를 받으면 이러한 조건들은 적용되지 않습니다.

저작권법에 따른 이용자의 권리는 위의 내용에 의하여 영향을 받지 않습니다.

이것은 [이용허락규약\(Legal Code\)](#)을 이해하기 쉽게 요약한 것입니다.

[Disclaimer](#)

A Thesis for the Degree of
Master of Science in engineering

**Numerical simulation of spatio-
temporal variation of red blood cell
aggregation under pulsatile flow**

JEJU NATIONAL UNIVERSITY
GRADUATE SCHOOL
Department of Ocean System Engineering

Cheong Ah Lee

2019. 08

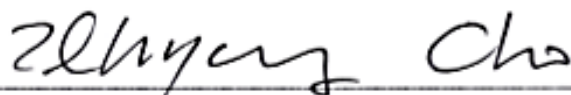
Numerical simulation of spatio-temporal variation of red blood cell aggregation under pulsatile flow

Cheong Ah Lee

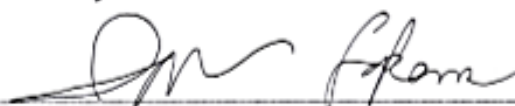
(Supervised by professor Dong-Guk Paeng)

A thesis submitted in partial fulfillment of the requirement for the degree
of Master of Science in Engineering
2019. 08

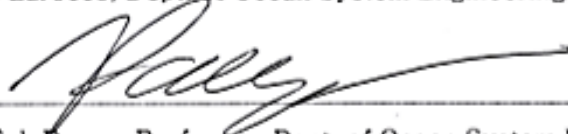
This thesis has been examined and approved by



Thesis director, Il-Hyung Cho, Professor, Dept. of Ocean System Engineering



John W. Larocco, Dept. of Ocean System Engineering



Dong-Guk Paeng, Professor, Dept. of Ocean System Engineering

Date 2019. 08

Department of Ocean System Engineering
GRADUATE SCHOOL
JEJU NATIONAL UNIVERSITY



Contents

초록(국문).....	iii
초록(영문)	vi
1. Introduction.....	1
1.1 Blood and red blood cells (RBCs).....	1
1.2 RBC aggregation.....	3
1.3 Previous Studies.....	7
1.4 Objective and Originality	9
2. Theory and Method.....	12
2.1 Theory.....	12
2.1.1 Mechanism of RBC Aggregation.....	12
2.1.2 Forces acting on RBCs.....	14
2.1.2.1 Interactional Forces.....	14
2.1.2.2 Hydrodynamic Force.....	16
2.1.3 Methodology and Solution of fluid.....	17
2.2 Simulation Approach.....	26
2.2.1 Numerical modeling of RBC Aggregation.....	27
2.2.2 Counting the Aggregated RBCs.....	31
3 Results.....	35
3.1 Simulation Under Steady flow.....	35
3.2 Simulation Under Unsteady flow.....	38
3.2.1 RBC aggregation Under Womersley flow.....	38

3.2.2	RBC aggregation Under Sinusoidal Pulsatile flow.....	42
3.2.2.1	RBC Aggregation Dependent on the Hemodynamic Variation.....	42
3.2.2.2	Quantitative Evaluation of the RBC Aggregation according to the Spatial Distribution of the Fluid Field.....	46
4.	Discussion.....	52
4.1	Analysis of RBC Aggregation Under Steady Flow.....	52
4.2	Simulation Under Sinusoidal Womersley Flow.....	53
4.2.1	Distribution of RBC Dependence on the Tube Wall under Womersley Flow.....	54
4.3	Simulation Under Sinusoidal Pulsatile Flow.....	56
4.3.1	RBC Aggregation Dependence on the Hemodynamic Variation.....	58
4.3.1.1	Velocity Amplitude.....	58
4.3.1.2	Mean Flow Velocity Dependence on RBC Aggregation.....	60
4.3.2	Quantitative Evaluation of the RBC Aggregation according to the Spatial Distribution of the Fluid Field.....	61
4.3.2.1	RBC Aggregation Dependence on Shear rate.....	62
4.3.2.2	RBC Aggregation Dependence on Flow Acceleration.....	65
5.	Limitation and Future works.....	66
5.1	RBC Properties.....	66
5.2	Analysis.....	66
5.3	Relationship between Acceleration and Shear rate.....	67
6.	Conclusion.....	68
7.	References.....	70

초록

이전의 실험 및 시뮬레이션 연구에서는 정상 유동에서 전단율이 낮을수록 적혈구 응집이 높아지는 반비례 관계가 알려져 왔다. 하지만 박동흐름에서 관찰된 파라볼릭 형태의 적혈구 응집은 전단율의 영향만으로 설명이 불충분하며 유체 가속도의 영향에 대한 가설이 제기되었다. 하지만 주기적으로 변화하는 압력에 의해 시, 공간적으로 복잡한 박동흐름의 속도장에서 적혈구 응집 현상을 실험으로 해석하기에 많은 제한점이 있다. 따라서 본 연구에서 2 차원 수치해석 시뮬레이션을 통한 적혈구 응집 현상을 관찰하였으며 박동흐름에서 시, 공간적 분포에 따른 적혈구 응집을 정성적 및 정량적 평가를 진행하였으며 탄성튜브에서 부피 보존을 만족시키는 워머슬리(Womersley) 유동에서 공간 변화에 따른 적혈구 응집 형성을 관찰하였다.

박동흐름에서 적혈구 응집의 2 차원 수치해석 모델링은 적혈구 입자 사이의 탄성력 및 응집력과 유체역학적 힘에 의해 각 입자의 운동이 계산되며 시간에 따른 움직임을 통해 응집 현상을 관찰하였다. 시뮬레이션은 유체의 진폭 및 평균 유속을 변화시켜 적혈구 평균 응집량을 계산하여 시간에 따른 적혈구 응집 변화량과 응집 정도를 정성적 평가했다. 또한 유동장의 공간 분포에 따라 영역 내 포함된 응집된 적혈구의 수를 계산함으로써 박동흐름에서 전단율 및 가속도

장에 따른 적혈구 응집의 정량적 분석을 진행하였다. 워머슬리 유동에서 공간 변화에 따른 적혈구 응집 형태의 차이를 확인하기 위해 강제와 탄성벽을 구현해 속도장의 공간변화가 적혈구 응집에 미치는 영향을 파악하였다.

본 연구 결과 박동흐름에서 유속 진폭이 증가할수록 평균 유속이 감소할수록 파라볼릭 형태의 적혈구 응집이 명확히 관찰됐다. 3 가지 응집 조건으로 구분지어 전단율 및 가속도 장의 공간 변화에 따른 응집된 적혈구 수를 측정한 결과 응집 발생 정도가 높을수록 전단율과 응집 사이의 반비례 관계 해석이 명확했으며 특정 가속도 구간에서 높은 적혈구 응집을 보였다. 이는 박동흐름에서 유변학적 인자로 전단율 뿐만 아니라 가속도도 적혈구 응집에 영향을 미친다는 사실을 확인했다. 워머슬리 흐름에서 공간 변화에 따른 적혈구 응집 분석은 속도장의 공간 변화가 없는 강제 튜브조건과 임의의 정현파 형태로 설계한 탄성튜브의 탄성 도를 조절하여 속도장의 공간 변화를 구현한 경우에서 적혈구의 움직임을 계산하였다. 시뮬레이션 결과 세 가지 힘에 의해 시간에 따라 달라지는 적혈구는 공간 변화가 없는 강제 튜브 내 적혈구 응집은 정상 유동에서 관찰된 적혈구 응집과 유사했으며 탄성 조건에서 속도장의 공간 변화에 따라 적혈구는 파라볼릭 형태의 응집 형성이 관찰되었다.

본 연구 결과는 박동흐름의 복잡한 시공간 변화에 대한 이해 향상을 목표로 적혈구 응집에 영향을 주는 세 가지 역학적 힘에 의한 수치해석 모델링을 수행하였다. 시뮬레이션을 통해 구현된 적혈구 응집 형태는 박동흐름에서 돼지 혈액으로 측정된 초음파 B 모드 이미지에서 관찰된 '백색환 (Bright collapsing ring)' 현상과 유사함을 보였다. 이 연구는 실험적 접근의 한계를 시뮬레이션을 통해 정량적 검증을 하였고 적혈구 응집체와 유체의 특성의 복잡성에 대한 이해를 향상시켰다.

Abstract

Previous studies on red blood cell (RBC) aggregation have elucidated the inverse relationship between shear rate and RBC aggregation under steady Poiseuille flow. From experimental studies under pulsatile flow, the effect of acceleration on RBC aggregation has been suggested to understand the insufficient relationship shear rate under steady flow. However, information on the cyclic and spatial variation in RBC aggregation under pulsatile flow remains lacking due to the complex interrelationship among the RBC motion and flow characteristics under pulsatile flow. In this study, the purpose of numerical 2 dimensional (D) simulation is that the spatial variation of the velocity field influence the RBC aggregation with interactional and hydrodynamic forces adopting elastic tube wall condition under pulsatile flow. RBC aggregation was numerically simulated to investigate the complex interrelationships among the parameters of RBC motion under pulsatile flow. Especially, the relationship between RBC aggregation and acceleration fields under pulsatile flow was quantitatively analyzed.

A 2D particle model was used to simulate RBC motion driven by hydrodynamic, aggregation, and elastic forces in a sinusoidal pulsatile flow field. The kinetics of

RBCs was simulated on the basis of the depletion model. The simulation was implemented to determine mean aggregation size as a function of time and the variation of the number of aggregated RBCs according to the spatial distribution of fluid fields. In addition, we observed the RBC aggregation with the spatial variation of velocity field by designing the elastic tube satisfying volume conservation under Womersley flow.

The simulation results are in agreement with previously observed experimental results for the formation and destruction of RBC aggregates with a parabolic radial distribution during a pulsatile cycle. In addition, the results demonstrated that the cyclic variation in the mean aggregate size of RBCs increased as velocity amplitude increased or mean flow velocity decreased under sinusoidal pulsatile flow in a rigid tube. In addition, it was confirmed that the spatial variation of the velocity field under Womersley flow depends on the degree of elasticity of tube walls and affects formation of RBC aggregation. The higher the elasticity of tube walls, the greater the spatial variation of velocity field with formation of a parabolic shaped RBC aggregation. In the spatial analysis of aggregated RBCs, the maximum aggregated RBCs occurred in a specific acceleration range.

The present simulation results verified previous experimental results and improved the current understanding of the complex spatiotemporal changes of RBC aggregates during a sinusoidal pulsatile and Womersley flow. The simulation results of RBC aggregation were similar to the Bright collapsing ring phenomenon obtained in the previous *in vitro* experimental results with porcine blood in ultrasound B-mode images. Mean aggregated size was simulated to show hemodynamic variation. The parabolic formation of RBC aggregation affected the spatial variation of velocity fields. In our simulation, we demonstrated the relationship between RBC aggregation and shear rate as well as acceleration of flow fields. The simulation results quantitatively verified previous experimental results and improved the understanding of the complex spatio-temporal changes experienced by RBC aggregates during pulsatile flow.

1. Introduction

1.1 Blood and red blood cells (RBCs)

The main role of blood is to supply the body tissues with oxygen from the lungs and nutrients absorbed from digestive organs. It also circulates in the body, carrying waste products produced from the cells [1]. Blood is consisted of red blood cells (RBCs), white blood cells and platelets, and about 55% components of plasma. Especially, RBCs in blood, also termed erythrocyte cells, play a role in the exchange of oxygen and carbon dioxide in tissues. As shown in Fig. 1, normal RBCs are biconcave disk shapes with a diameter of 7.5-8.7 μm , a center thickness of 0.8 μm and an edge thickness of 2.6 μm [2]. The biconcave shape of the RBCs maximize the cell surface area, allowing sufficient gas exchanges in the tissue [3]. In addition, it is well known that RBCs not only play a role of gas exchange in the tissue, but also change the viscosity of blood by aggregation of RBCs at lower shear rate. This means, non-Newtonian fluid in the blood flow dynamics were affected by the physiological and biochemical behavior of RBCs. Based on the interpretation of the relationship between RBC aggregation and hemodynamic characteristics, prediction and diagnosis of circulatory diseases may be possible. The

hemorheologic factors for analyzing pathologic phenomena depend on RBC aggregation, red cell deformation, whole blood viscosity and plasma viscosity [3].

In this paper, we investigated RBC aggregation among these hemorheologic factors.

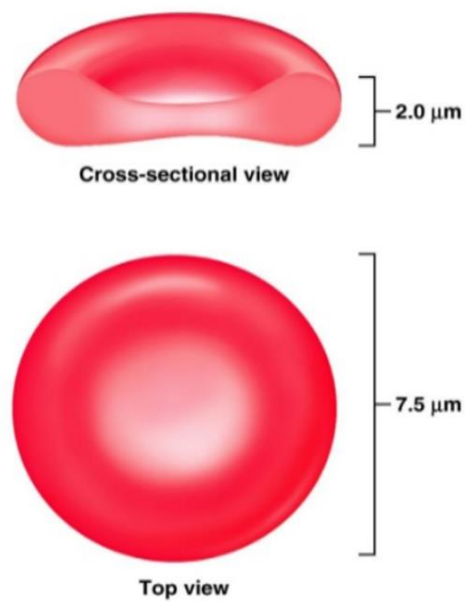


Fig. 1 Normal Red blood cells morphology. Fig. 1 shows the single biconcave shape of RBC and radial size from the cross sectional and top view [53].

1.2 RBC aggregation

RBC aggregation occurs when RBCs are stacked under low shear rate and formed a pile or network mediated by macromolecules such as protein and fibrinogen in plasma, called rouleaux [4]. Fig. 2 represents the non-aggregated RBC particles and RBC aggregation [4,5]. The aggregated RBCs form a linear or long-linear structures.

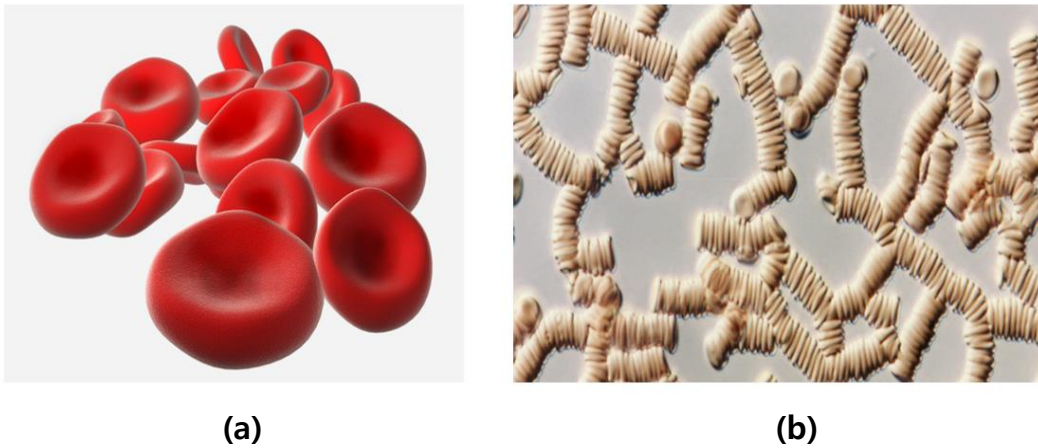


Fig. 2 Shape of RBCs. Fig. 2(a) shows the non-aggregated RBCs [5] and Fig. 2(b) represents the aggregated RBCs, which is formed linear structure termed a rouleau [4].

The non-Newtonian fluid behavior of whole blood is dependent on shear rate. RBC aggregation is also determined by shear rate. Many investigators demonstrated that the behavior of RBCs in whole blood was related to viscosity and shear rate in both *in vitro* and *in vivo* experiments [6-9]. As depicted in Fig. 3, low shear rate down to 0.1 s^{-1} indicated high RBC aggregate level with high

viscosity in normal cells in plasma. At high shear rate over 100 s^{-1} , a little change in viscosity is observed and the effect of deformation is greater than RBC aggregation [1]. Normal cells without fibrinogen are hardly affected by the RBC agreeability in shear rate. In addition, hardened cells in plasma are not affected by the degree of aggregation and deformation of the RBCs. In other words, it is a Newtonian fluid of constant viscosity with shear rate without the RBC aggregation and deformation.

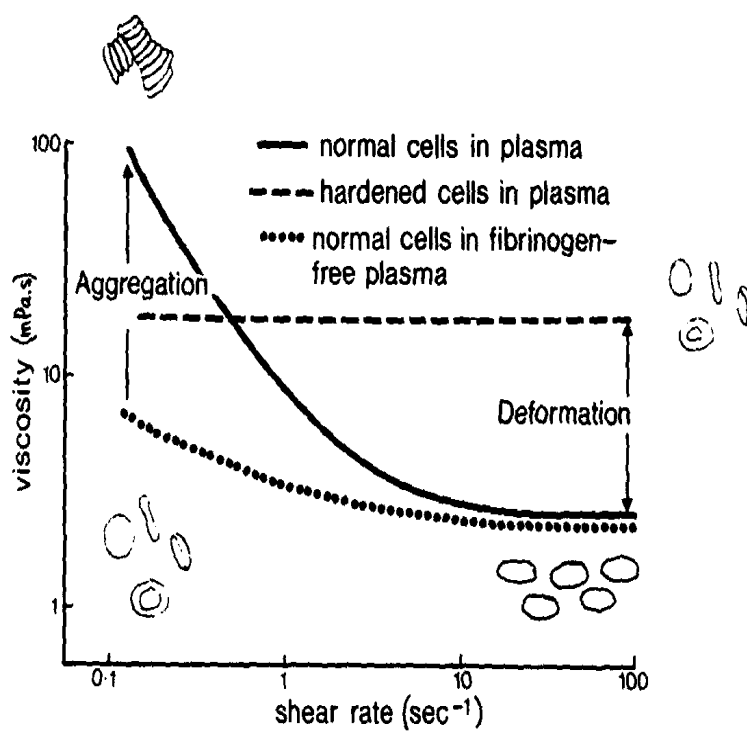


Fig. 3 Relationship between the viscosity and shear rate in the blood. A comparison of the viscosity and shear rate relationship of blood components in three conditions, which consists of the normal cell (solid line), hardened cell (broken line) and normal cells without the fibrinogen (dotted line) in plasma [1].

Excessive aggregation of RBCs in low shear rate is an important indicator for diagnosing some cardiovascular diseases [4,10-12]. Abnormal RBC aggregation, which is the main factor to increase viscosity, was measured as high aggregated levels in patients with myocardial ischemia and heart disease [13-15]. Since the nineteenth century, microscopic observation of blood samples have served as a method to detect the degree of the RBC aggregation [4,16]. In Fig. 4, the rouleaux formation shows the different between normal and RBC aggregation of diseased

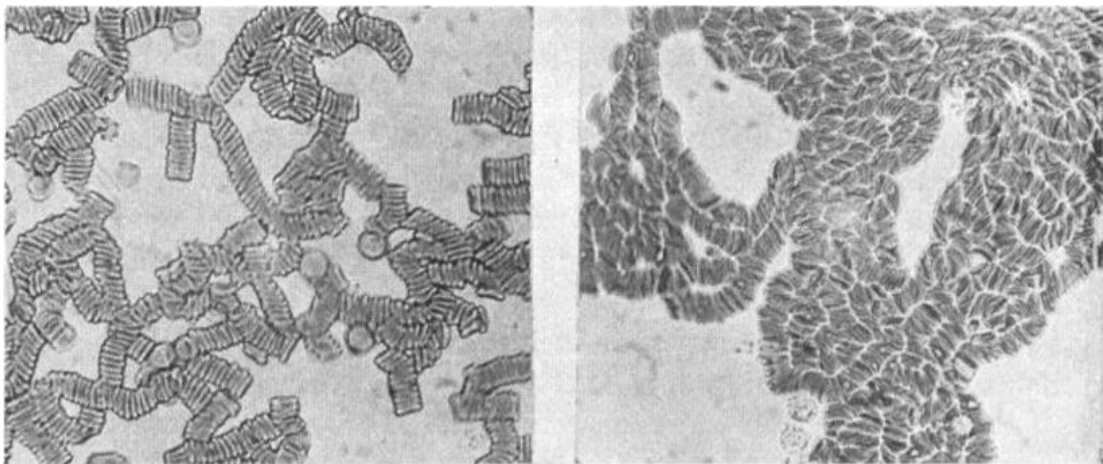


Fig. 4 Microscopic observation of the rouleaux in normal and pathological blood [16]

person [16]. The rouleaux in pathological blood are clustered to a high degree and formed larger structures.

Compared with normal subjects, the patients with angina pectoris and ischemic heart disease have higher whole blood viscosity [17,18]. In the relationship between hypertension and RBC aggregation, it has been widely accepted that hypertension is relevant to increasing the viscosity in whole blood and formation of RBC aggregation. [10,19]. A study reported the relationship between RBC aggregation and hypertension from evaluation in 320 patients to improve the clinical and therapeutic approach to treatment of arterial hypertension. The results observed in the patients with hypertension showed that the rheological and biochemical characteristics of RBCs in blood flow were affected by RBC aggregation [19]. Understanding of RBC aggregation is important not only in cardiovascular disease but also in systemic inflammation. The quantitative measurement of the RBC aggregation is potentially an inflammatory blood marker in a critical care situation [20]. Consequently, many experimental and computational studies for RBC aggregation have been performed to understand the rheological mechanism of RBC aggregations.

1.3 Previous Studies

Robin Fåhæus was the first scientist to prove the importance of RBC aggregation in tube flow [16]. Since then, many studies have been done on the relationship between RBC aggregation and fluid properties. The properties of the flowing fluid influenced the RBC aggregation and red cell deformation. Several experiments were performed to observe the effect of the blood viscosity in a glass tube. The early reports indicated that the viscosity of blood was observed to increase at lower flow rate [4]. It is mainly revealed that direct or microscopic observation of RBC aggregation properties were dependent on the blood flow dynamics in tube flow. It was also suggested the formation of a marginal RBC cell poor layer during the blood flow in the early 1900s [21]. In the studies under steady Couette and Poiseuille flow, shear rate could be easily controlled and well defined as the inverse relation between viscosity and shear rate.

An experimental study has been conducted on porcine whole blood to verify the tendency of RBC aggregation as a function of mean shear rate under steady flow. The results suggest that the RBC aggregation tendency of porcine whole

blood is similar to that of normal human blood and disaggregation of the RBC at high shear rate [22]. In other experiments, echogenicity was observed in a vertical tube using a Doppler probe under steady flow of mean shear rates across the tube between 8.5 and 102 s^{-1} . For porcine whole blood, the results were presented that an angular dependence exist and viscosity is a function of the shear rate [23].

Other studies have also been conducted under pulsatile flow using ultrasound B-mode imaging [7,24-27]. In previous studies, the 'bright collapsing ring (BRCR)' phenomenon, which is a bright echogenic ring converging from the tube wall and finally collapsing near the tube center during a pulsatile cycle in cross-sectional B-mode images [28,29], was observed from porcine blood and human carotid artery [30]. The phenomenon was investigated that cyclic and radial variations in echogenicity were dependent on peak blood flow speed at systole, stroke rate, and mean steady flow under pulsatile flow [28,29]. In our previous study, the numerical simulation under the sinusoidal pulsatile flow based on depletion theory demonstrated the complex interrelationships among the parameters of RBC motion from interactional and hydrodynamic forces. The simulation results showed the formation and destruction of RBC aggregates with a parabolic radial

distribution during a pulsatile cycle [31].

Although the dynamic process of RBC aggregate formation was in agreement with the results of the *in vitro* porcine blood experiments with BRCC phenomenon, these results suggest that the relationship between shear rate field and RBC aggregation was not yet fully understood under pulsatile flow. Velocity field under pulsatile flow is complex because it changes in the length of the tube and in the radial direction. Ultimately, it is necessary to analyze RBC aggregation considering the spatial distribution under pulsatile flow.

1.4 Objective and Originality

RBC aggregation is affected not only by temporal variation but also by spatial changes. Many previous studies have observed the characteristics of RBC aggregation with radial variation under steady flow. Under pulsatile flow, a few studies were analyzed as a view of temporal variation [24,28,29,31,32]. However, pulsatile flow has a different velocity profile in the radial and longitudinal directions of the tube. Therefore, the velocity profile in longitudinal direction under pulsatile flow may affect the RBC aggregation. However, the RBC aggregation in longitudinal

direction is complex and difficult to study through the experiments. From several experimental results under pulsatile flow, the interrelationship among RBC aggregation and shear rate was not clearly explained. A hypothesis concerning the combined effects of shear rate and flow acceleration under pulsatile flow was suggested as an explanation of the cyclic and radial variation of echogenicity [33]. The quantitative analysis to support the hypothesis has not been provided yet due to the complexity of the spatio-temporal distribution of RBC aggregation.

In this research, we investigated the interrelationship among RBCs in their aggregation mechanism and spatio-temporal variation of RBC aggregation under sinusoidal pulsatile flow. First, we described qualitative results of RBC aggregation during a cyclic under pulsatile flow. Then we quantitatively analyzed to investigate the relationship between the RBC aggregation and flow acceleration field through the spatial and temporal distribution of RBC aggregation under sinusoidal pulsatile flow in a 2-dimensional tube based on the depletion model.

To verify spatial analysis of aggregated RBCs, it was attempted to validate the results from the pulsatile flow based on the steady flow condition in this simulation

model. Under steady Poiseuille flow, the effect of shear rate on RBC aggregation was validated through a numerical simulation method. Then shear rate and acceleration fields under sinusoidal pulsatile flow velocity profile were analyzed to show the spatial distribution of aggregated RBCs. This study focused on how shear rate and flow acceleration affect the spatial distribution of aggregated RBC during pulsatile flow cycles.

2. Theory and Method

2.1 Theory

In this section, we explain a theoretical description of two coexisting theories, namely bridge model and depletion model, and the related forces acting on the RBCs. RBCs aggregate and form rouleaux due to interactional and hydrodynamic forces. We describe mathematical theories about the forces acting on these RBCs. Characteristics of blood flow are considered under steady and un-steady flow conditions based on hydrodynamic forces, and the definition and formula of the fluid applied to the numerical simulation are specified.

2.1.1 Mechanism of RBC Aggregation

Although studies on RBC aggregation have been ongoing for decades, the mechanism of RBC aggregation has not yet been fully elucidated. There are two mutually exclusive, but coexisting hypotheses, bridging model and depletion model, which are commonly known for RBC aggregation.

In a study at the single cell level, the mechanics of RBC interaction between RBCs were found that the adjacent cell surfaces in the rouleaux were parallel to each other with a rather uniform intercellular distance [34]. Therefore, those results led

to mechanism of RBC aggregation from macromolecular bridging phenomenon. The bridging model proposed that RBC aggregation occurs to cell-cell, when bridging forces due to the adsorption of large macromolecules onto adjacent surfaces of each RBC cell exceed disaggregating force due to electrostatic repulsion, membrane strain and mechanical shear effects [4,35]. When the RBC aggregation occurs, dynamic deformation related to electrical repulsive force and surface strain lead to intercellular attraction due to adsorption of macromolecules.

The opposing theory to the above aggregation mechanism is the depletion model. In this model, RBC aggregation due to a lower localized protein or polymer concentration near the cell surface. When the surfaces of the RBCs contact to each other, the RBC aggregation is caused by a sudden change of the osmotic pressure in the intercellular medium [36]. Then, the polymer-reduced space between the two surfaces is decreased by attractive force. Fig. 5 represents rouleau formation by the two coexisting mechanisms. Fig.5(a) is a snapshot of a rouleau [37]. Fig. 5(b) shows the cross-section of RBCs in the bridging model. Fig.5 (c) illustrates the RBC aggregation mechanism with depletion model. This model demonstrates the change in osmotic pressure by maximizing the contact area (yellow area) between

the RBC particles, as opposed to the bridge model required by the dynamic deformation. In this research, the numerical simulation model for the RBC aggregation was based on the depletion model.

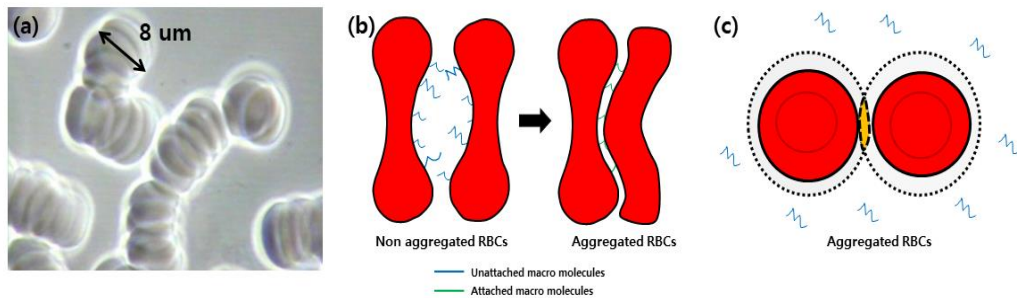


Fig. 5 Two coexisting mechanism of RBC aggregation. Fig.5 (a) from reference [37]. Snapshot of a rouleaux observation of microscopic. Fig.5 (b) and Fig.5 (c) are schematic illustrations of the bridging model and the depletion model, respectively.

2.1.2 Forces acting on RBCs

2.1.2.1 Interactional Forces

It should be noted that the interactional forces determined by summation of the elastic force (f_{ij}^e) and the aggregation force (f_{ij}^a) are theoretically calculated based on the depletion model. The RBC aggregate between two RBC particles is a function of distance.

The elastic force (f_{ij}^e) based on a granular interaction model acting on the two particles is applied only when the distance between two particles is smaller than the diameter of an RBC in Equation (1).

$$f_{ij}^e = \begin{cases} k(2R - d)^{\frac{2}{3}}\mathbf{n}, & \text{if } d < 2R \\ 0, & \text{otherwise} \end{cases} \quad (1)$$

where d indicates the distance between the centers of mass of two RBCs, R is the radius of an RBC particle, and \mathbf{n} is the normalized vector from one RBC to the other.

RBCs are not considered rigid and compressed by the factor modulated by 3×10^6 N/m of the elastic modulus (k). When the distance between the centers of two RBCs is smaller than the cell diameter $2R$, the elastic force acted on the two particles.

The aggregation force is derived by the depletion layer thickness between cell to cell distance [36,38,39]. We considered the depletion theory developed by Neu and Meiselman. Equation (2) was adapted from the literature by Fenech et al [36,38] for the aggregation force condition. The interaction energy between RBCs in polymer solutions is calculated using Morse potential in Equation (3).

$$f_{ij}^a = 2DAB(e^{2B(\delta_0-\delta)} - e^{B(\delta_0-\delta)})\mathbf{n} \quad (2)$$

$$\Phi_{ij} = D(e^{2B(\delta_0-\delta)} - 2e^{B(\delta_0-\delta)}) \quad (3)$$

where D is a coefficient of surface energy and A indicates the area of RBC surface in cell-cell apposition with another cell. DA and B are respectively the energy and a scaling factor, which is inversely related to depletion layer thickness. δ is the cell

membrane distance between two RBCs ($\delta=d-2R$). δ_0 is the δ for which the aggregation force is zero. In this paper, the constant values of DA , B and δ_0 are 10^{-25} J, 107 m^{-1} and 11 nm respectively.

2.1.2.2 Hydrodynamic Force

Previously, we mentioned the interaction forces between RBC particle (i) and the other RBC one (j). In case of flowing fluid, it is known that not only the viscous properties of the fluid but also the variation of spatio-temporal distribution of the flow field affects the movement and aggregation of the RBCs. For example, the dynamical properties of RBCs are different under steady Poiseuille flow or un-steady pulsatile flow. Therefore, we considered the hydrodynamic force as a force that can affect the motion and interaction of RBCs. In the following paragraph, we describe equations and conditions for the forces acting between the fluid and RBCs.

Basset found the hydrodynamic force acting on a spherical particle undergoes arbitrary time-dependent motion in an otherwise quiescent fluid [40]. In Equation (4) the hydrodynamic force consists of three terms. The first term is called as the pseudo-steady Stokes drag force, which depends on the past history of the particle motion. The second term on the right hand side of the equation includes viscous

force and inertial force, termed as a Basset memory integral. However, the second term can be neglected because the Reynolds number is much less than one. In the last term on the right hand side of Equation (4), the added mass force is dependent on the concentration and size of the particle. The Stokes drag force is much larger than the added mass force, so that inertial force by added mass can be neglected. Basset's result [40] is the summation of these three forces in Equation (4):

$$f_i^h(t) = -6\pi\mu R U_p(t) - 6\pi\mu R \left(\frac{R^2}{\pi\nu}\right)^{\frac{1}{2}} \int_{-\infty}^t \frac{\dot{U}_p(s) ds}{(t-s)^{\frac{1}{2}}} - \frac{2}{3} \pi\rho R^3 \dot{U}_p(t) \quad (4)$$

where $U_p = U_0 - U_i$, U_0 is the velocity of fluid in the absence of particles and U_i is the particle velocity. μ and ν are the dynamic and kinematic viscosities of blood, respectively. ρ is the density of blood cell. Definitions and explanations of the fluids in the hydrodynamic forces are described in detail in the following session.

2.1.3 Methodology and Solution of fluids

2.1.3.1 Methodology

In this research, we focused on three themes: simulation verification, qualitative and quantitative evaluation of RBC aggregation by spatio-temporal distribution. To

set the stage for the hydrodynamic force in this simulation, Equation (4) is simply expressed as an Equation (5):

$$f_i^h(t) = -6\pi\mu R\{U_0(x, y, t) - U_i(x, y, t)\} \quad (5)$$

where $U_0(x, y, t)$ is the velocity of the fluid in the absence of particles, and $U_i(x, y, t)$ is particle velocity. In the analysis of the flow in a 2D tube, the y direction in the Cartesian coordinate system represents the radial direction of the tube, the x direction is defined as a tube length direction, and the z direction was not considered. The dynamic viscosity is 2.7×10^{-3} Pa.s [31].

(1) Steady Poiseuille flow

We observed the RBC aggregation phenomenon under steady Poiseuille flow, which is less complex to evaluate accurately for verification of numerical simulation modeling based on experimental data. The variation in time is not considered, so the hydrodynamic force depends on the y axis alone. In addition, spatial velocity gradient in the x direction is 0, and the spatial gradient in the y direction has a constant value. It is relatively easy to analyze the characteristics of aggregated RBCs according to the spatial distribution under steady Poiseuille flow, considering

the variation of velocity in the y direction alone. We applied the velocity profile in Equation (6) to Equation (5) in order to analyze the RBC aggregation as a function of the mean shear rate.

Profiles of the velocity and shear rate were as following:

Steady Poiseuille flow ($U(y)$) driven by external pressure gradient force is described as the parabolic velocity profile in Equation (6).

$$U(y) = A_o \left(1 - \frac{4}{h^2} y^2\right) \quad (6)$$

where A_o and h indicate the amplitude of flow and tube diameter, respectively.

Shear rate profile is described in Equation (7), and the shear rate profile can be easily induced,

$$SR(y) = \frac{d}{dy} U(y) = -A_o \frac{8y}{h^2} \quad (7)$$

where $SR(y)$ is derived as a constant gradient in the y direction. The range of mean shear rate was governed by direction of diameter (y) and amplitude of fluid (A_o).

(2) Womersley Flow

Many studies in the experiment and simulation have investigated the relationship between the RBC and behavior of fluid with cyclic variation because the analysis of the RBC aggregation by spatial distribution is complex and limited. This paper hypothesizes that the spatial variation of the velocity field is a factor to influence RBC aggregation. Therefore, we have adjusted the elasticity of the wall of the tube to satisfy the volume conservation to consider the spatial distribution of the velocity field under Womersely flow.

It is well known that Womersley flow (or oscillatory flow) was derived by John R. Womersley with the blood flow in the arteries [41]. The non-steady Womersley flow has been solved to obtain an analytical solution of Navier-Stokes equation in the tube. Thus, the Navier-Stokes equation and the continuity equation are simplified as following:

$$\rho \frac{\partial u}{\partial t} + \left(u \cdot \frac{\partial u}{\partial x} \right) = - \frac{\partial P}{\partial z} + \mu \left(\frac{\partial^2 u}{\partial x^2} + \frac{\partial^2 u}{\partial y^2} \right) \quad (8)$$

where, u is velocity profile of non-steady oscillating flow condition with rectangular cross section with x and y direction in Equation (8). ρ is the fluid density (1060 kg/m³ for a human whole blood average density) and μ is the dynamic

viscosity (2.7×10^{-3} Pa.s) We assumed that the fluid is homogeneous and incompressible. By assuming a transverse velocity component of $u(x,y,t)$ with cross section, we imposed across to flow field with an oscillating pressure gradient in the z-direction in Equation (9).

$$\frac{1}{\rho} \frac{\partial P}{\partial z} = -P_0 e^{i\omega t} \quad (9)$$

The pressure gradient driven flow is represented by Equation (9). P_0 is the imaginary amplitude of imposed pressure gradient during periodic function of the time with the cyclic frequency (ω) of the oscillation.

In this reference [42], a solution to the velocity profile in the cross-section of the flow in a rigid tube under Womersley flow was solved in a rectangular coordinate system. The boundary condition of the no-slip with x and y axis was applied to the wall of the tube. It is noted that the velocity profile in the rectangular rigid tube was computed in a Cartesian coordinate, which results in a simple sinusoidal velocity profile, differs from the method of solving the velocity profile in a cylindrical pipe such as vessel. Since our purpose is to analyze the force acting between the fluid and particles from a macroscopic point of view, our simulation

adopted the velocity profile in rectangular tube under Womersley flow.

$x = \pm\lambda$, the final solution is as following:

$$U(x, y, t) = \frac{4}{\pi} \sum_{n=0}^{\infty} \frac{(-1)^n}{(2n+1)p^2} \left\{ 1 + \frac{1}{\sinh(D\lambda)} \left[e^{\frac{Re+D}{2}x} \times \sinh\left(\frac{Re-D}{2}\lambda\right) - e^{\frac{Re-D}{2}x} \times \sinh\left(\frac{Re+D}{2}\lambda\right) \right] \right\} \cos\left(\frac{(2n+1)\pi}{2}y\right) e^{i\omega t} \quad (10)$$

$$\text{where } \beta = \sqrt{w/v}, \quad p^2 = i\beta^2 + \left(\frac{(2n+1)\pi}{2}\right)^2, \quad D = \sqrt{Re^2 + 4p^2} \quad (11)$$

In Equations (10) and (11), the w is wave angle and β is a dimensionless variable, which is expressed as the ratio of wave angle (w) and kinematic viscosity of blood (v). Equation (10) is obtained by the superposition of the non-steady velocity profile in a rectangular duct with 0 of Reynolds number (Re). However, our purpose is to analyze RBC aggregation by temporal and spatial changes in the longitudinal view. Therefore, in the velocity field of the cross section in Equation (10), the velocity component in the y direction was extracted at the center of the tube in the x direction as shown in Fig. 6(a) and (b). Fig. 6(b) shows the real (left) and the absolute value (right) component of the velocity field. We extracted the velocity components from the solid black window and applied to the longitudinal tube length. Fig. 6(c) represents the velocity field in ROI as a function of time. The

obtained velocity component is assumed to be un-steady flow, but there are no

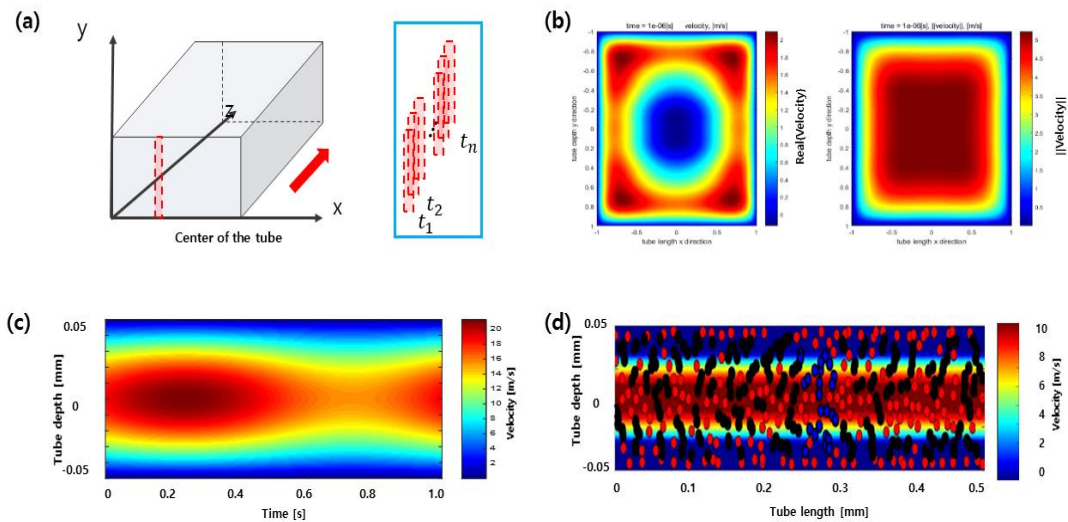


Fig. 6 Process of the extraction of longitudinal velocity field from the un-steady Womersley flow at the cross sectional velocity field. Fig 6(a) is schematic illustration of measuring the cross sectional velocity field under the Womersley flow. Fig. 6(b) represented the real (left) and absolute (right) value of the velocity field at the same time. Fig. 6(c) is velocity obtained in the window as a function of the time. Fig. 6 (d) shows the RBC aggregation under un steady Womersley flow field. The velocity field is similar to the steady flow at the spatial distribution, respectively.

spatial changes in the direction of the tube length. Finally, the velocity fields were applied to RBC aggregation modeling. In Womersley flow, we assumed an elastic tube condition to apply the spatial variation of the pulsatile flow. In other words, the spatial variation of the velocity field was calculated by arbitrarily adjusting the elasticity on the tube wall.

(3) Sinusoidal pulsatile flow

In this research, the numerical simulation has focused on the RBC aggregation under sinusoidal pulsatile flow with a single frequency component for quantitative evaluation of RBC aggregation with the temporal and spatial variation.

Sinusoidal pulsatile flow is defined as a combination of Poiseuille flow in the y -axis and sinusoidal velocity profile traveling with a certain speed in the x -axis in Equation (12) [31].

$$U(t, x, y) = \{A_f \sin(\omega t - k_f x) + B_f\} \left(1 - \frac{4}{h^2} y^2\right) \quad (12)$$

A_f and B_f are the amplitude of velocity and mean flow velocity, respectively. In the sinusoidal wave term, k_f is the wave number and ω represents the angular frequency traveling along the x -axis with the hydrodynamic conditions (velocity amplitude and mean flow velocity).

$$SR(x, y, t) = \frac{\partial}{\partial y} U(t, x, y) = \{A_0 \sin(\omega t - k_0 x) + B_0\} \left(\frac{8y}{h^2}\right) \quad (13)$$

$$a(x, y, t) = \frac{\partial}{\partial t} U(t, x, y) = A_0 \omega \sin(\omega t - k_0 x) \left(1 - \frac{4}{h^2} y^2\right) \quad (14)$$

In the sinusoidal pulsatile flow, shear rate profile is induced by the velocity gradient

in y axis in Eq. (13). The velocity gradient over time represents flow acceleration field of the sinusoidal pulsatile flow, and the expression was given by Eq.(14). In Eq. (13) and (14), the velocity gradient over space (Eq. 13) and time (Eq.14) was dependent on the x and y components under pulsatile flow during a cycle. Fig. 7 is a snapshot of the shear rate and acceleration field derived from the pulsatile flow at the same time. Fig. 7(a) represents the velocity field with hydrodynamic characteristics of amplitude 1.5 mm/s and 2 mm/s of mean flow velocity. Unlike the Poiseuille flow with change along the radial direction alone, shear rate (Fig.7(b)) and acceleration field (Fig.7(c)) vary with space and time, so that it is difficult to interpret the pulsatile flow.

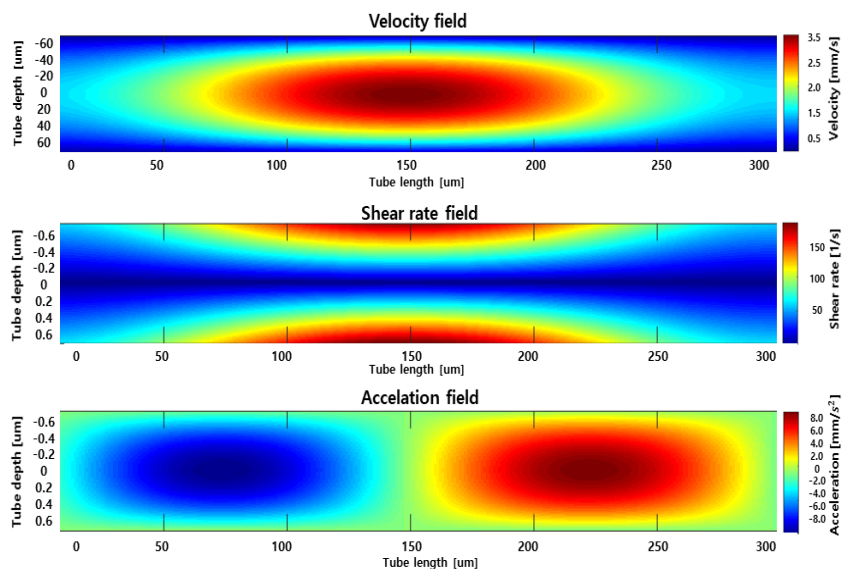


Fig. 7 A snapshot of the velocity, shear rate, and acceleration field at the same time. Fig.7 (a) show the velocity field of the sinusoidal pulsatile flow with 1.5 mm/s of velocity amplitude and 2 mm/s of mean flow velocity. Fig.7(b) and (c) represent the spatial and temporal change gradient derived from the field of velocity under the pulsatile flow.

2.2 Simulation Approach

In Chapter 2.2, we provide description of the basic theory based on numerical simulation modeling for analyzing RBC aggregation. An approach of the numerical simulation model is to calculate the velocity and location of initially disaggregated RBCs travelling along streamlines of flow field in a 2-dimantional rigid or elastic tube, and then to track the spatial distribution of aggregated RBCs in each shear rate and acceleration field.

2.2.1 Numerical modeling of RBC Aggregation

Fig. 8 illustrates the numerical approach of RBC modelling by the following procedure of three steps. First, we set the flow condition (select the steady flow or pulsatile flow) and the RBC properties as shown in Fig. 8 (A. initial condition). The properties (shape, size, and density) of RBC particles are circles of equivalent radius of $4 \mu\text{m}$ and mass of 2.94×10^{-13} kg. The total number of RBCs (238 particles), which is equivalent with 40% hematocrit, were randomly distributed without aggregation throughout two-dimensional space with a diameter of 0.1 mm and a tube length of 0.3 mm.

The interactional forces (f_{ij}) between RBC particles i and j and hydrodynamic force (f_i^h) are important in determining whether RBCs form aggregate or not. As shown in Fig.8 (B. RBC motion), the second step is to calculate the interactional forces between two particles and hydrodynamic force among RBCs and flow. In this simulation, the RBC particles were driven by those three forces of Newton's second law. The acceleration of an RBC particle i over time t is given in Eq. (15) and (16) [38]

$$m_i \frac{dv_i}{dt} = \sum_{i \neq j} f_{ij} + f_i^h \quad (15)$$

$$f_{ij} = f_{ij}^a + f_{ij}^e \quad (16)$$

Based on the Newton's second law, the distance (d_i), velocity (v_i), and acceleration (a_i) of an RBC particle (i) were calculated as a function of time.

In the simulation, we imposed the cyclic boundary condition in the flow direction as follows: each particle leaving the right side was positioned at the left entrance at the same y -coordinate with the same acceleration, velocity and force vectors. The details of RBC position and motion were described in our previous study [31]. It should be noted that the flow is treated as incompressible viscous flow and the RBCs are rigid spheres without any deformation, which is different from the reality in the above theoretical solutions. The time step utilized at each iteration was selected to meet maximal displacements for all RBCs to be smaller than half of the tube length. RBC aggregation kinetics was described by the mean aggregate size (MAS) variation as a function of time.

This simulation was undertaken to provide a basis for relationship between RBC aggregation and spatial distribution of shear rate of flow. Therefore, the last step

as shown in Fig. 8 (C. processing) is the analysis of the distribution of aggregated RBCs as follows:

(1) The velocity field was calculated according to the flow properties selected in step (A, initial condition), and the shear rate and acceleration fields were derived from the velocity fields. It is noted that the velocity amplitude and mean flow velocity were decided by the range of shear rates approximately less than 180 s^{-1} .

(2) The window for observing aggregated RBCs should be designed. The ROI was implemented in two ways depending on whether spatial change was considered (supplementary description in Chapter 2.2.2).

(3) We qualitatively and quantitatively evaluated the interpretation of aggregated RBC and rheological relationships in the selected ROI.

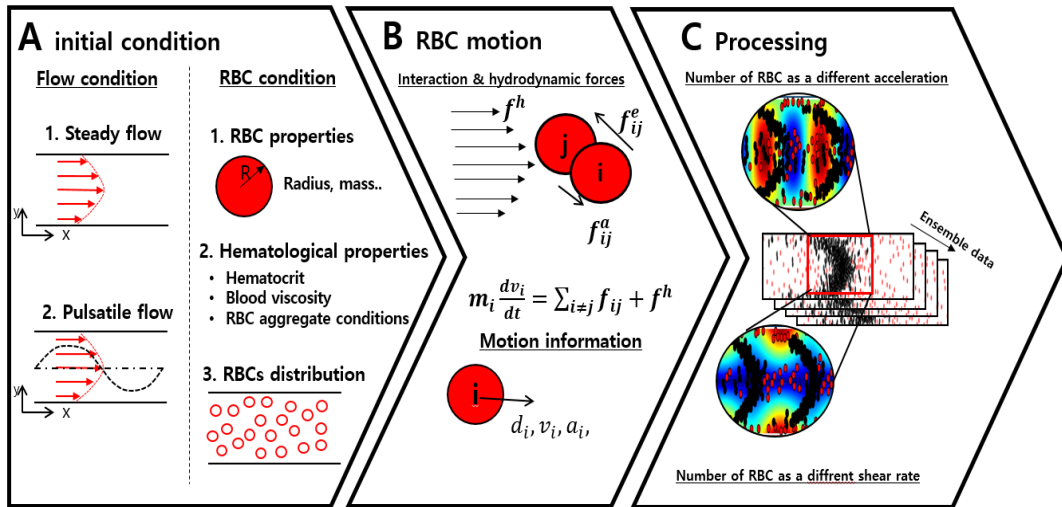


Fig. 8 Flow chart of mechanisms to analyze red blood cell (RBC) aggregation under sinusoidal pulsatile flow. The simulation consists of three steps. First, the simulation controls flow characteristics and both RBC properties and tube conditions such as tube diameter and tube length. Second step is to calculate the three forces that affect RBCs and to judge the movement and aggregation of RBCs during the time. Finally, the final step consists of analyzing RBC aggregation as a function of the time and spatial distribution of fluid characteristics.

2.2.2 Counting the Aggregated RBCs

It is necessary to observe spatial and temporal changes in RBC aggregation. Specifically, the count of the number of RBC aggregates is a criterion to evaluate the relationship between spatial and temporal distribution and the RBC aggregation. In this session, we mention two methods for measuring the aggregated RBCs in a specific region of interest (ROI). A mean aggregation size (MAS) approach focuses on the evaluation of the mean aggregate as a function of the time in ROI that does not consider the spatial variation. Conversely, there is a purpose to quantitatively evaluate the effect of spatio-temporal variation by counting the number of aggregated RBCs in the ROI considering the spatial distribution.

(1) Mean Aggregation Size (MAS)

MAS is the number of mean aggregates in an ROI. That is, MAS can be calculated as the ratio of the total number of aggregated RBC particles to the number of RBC aggregate in the ROI. This is a method for evaluating the amount and variation of MAS according to the hydrodynamic characteristics during the time. Fig. 9 shows RBC aggregation distribution. (Fig.9(a)) shows the corresponding velocity field to

(Fig.9(b)) in the 2D tube at a certain time. The particles visualized in black are aggregated RBCs in the ROI (0.1 mm x 0.1 mm). It should be noted that the calculation for value of velocity in the ROI assumes a velocity measured at the center in the radial direction of the tube without spatial variations of the velocity field.

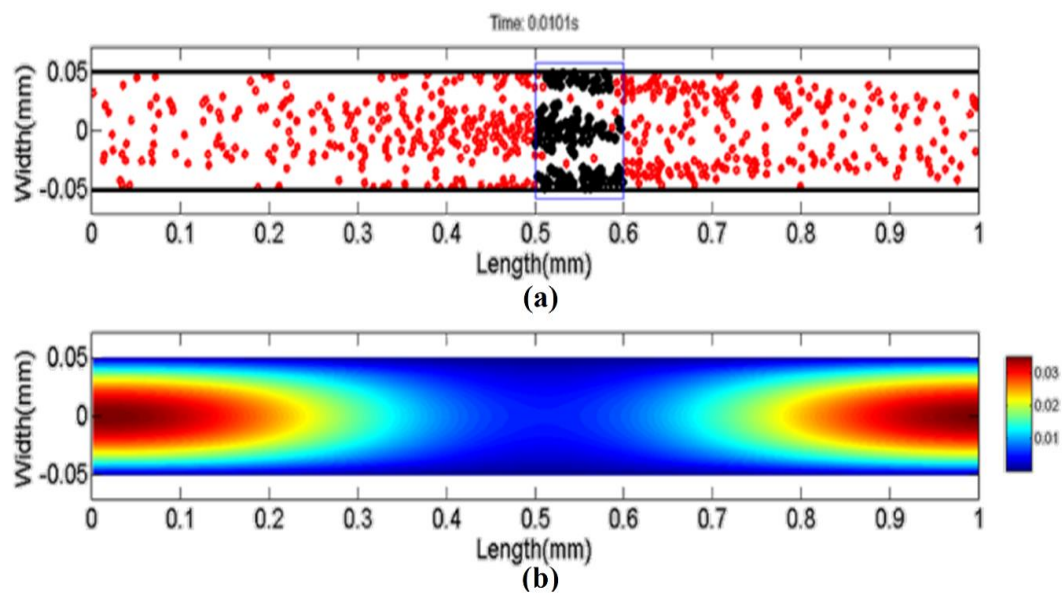


Fig. 9(a) Distribution of 596 RBC particles at a hematocrit of 30% at one time point. The black particles represent RBC aggregation in a field with dimensions of $0.1\text{ mm} \times 0.1\text{ mm}$, where MAS was analyzed with the given hemodynamic parameters. Fig. 9(b) Velocity profile of pulsatile flow combined with Poiseuille flow and steady flow under the velocity amplitude (A) of 1 cm/s and the steady mean flow (B) of 2 cm/s. The color bar represents velocity in m/s.

(2) The number of aggregated RBCs

In considering the temporal and spatial changes, it is not right to calculate MAS in the same ROI approach because the RBC aggregates are affected by temporal and spatial variation of the fluid. Therefore, as shown in Fig. 10, the flow field is divided into regions of having the same value. In this case, each value is divided into having the same area. Finally, the number of aggregated RBCs contained in each ROI was counted. Fig. 10(a) shows the shear rate field with 10 divided areas. The same mean shear rate areas were indicated as a white solid line and the shear rate was axisymmetric. Fig. 10 (b-e) shows a process of calculating the number of aggregated RBCs in each 10 ROI.

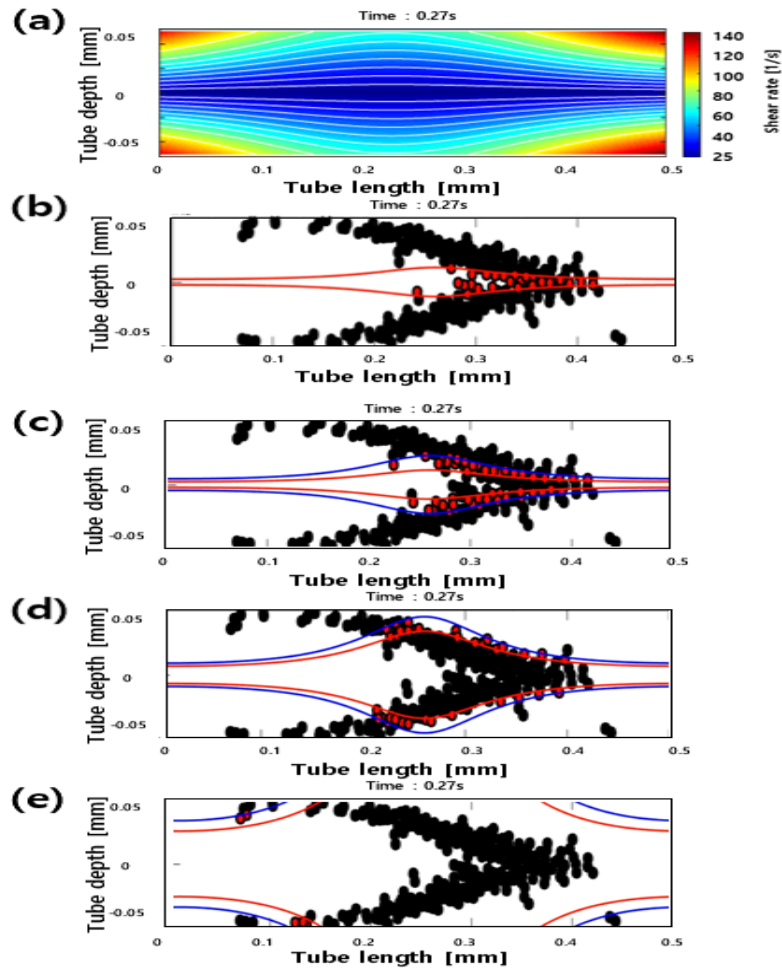


Fig. 10 In the shear rate field, the process of counting the number of aggregated RBCs contained in each ROI of the same area with the same mean shear rate. Fig. 10(a) represents the axial symmetry shear rate divided by 10 regions with the same area and same mean shear rate. Divisions of segment were white solid lines. Fig. 10(b-e) show the process of counting the number of aggregated RBCs in the ROI with the spatial distribution at the same time.

3. Results

3.1 Simulation Under Steady Flow

In order to determine the accuracy of our modeling for the analysis of the relationship between shear rate and RBC aggregation under pulsatile flow, we first checked the results of RBC aggregation as a function of the mean shear rate under steady flow in a shear rate range similar to that measured in other experiments [43-46]. For the process of an iteration, this simulation adopted the velocity profiles in Eq. (6) with different flow amplitudes 2, 3, and 5 mm/s. In Fig. 11, each of the symbols represents the mean values of 50 samples derived from the number of aggregated RBCs as a function of the mean shear rate for the three conditions. The simulation results show that the apparent RBC aggregation decreases with mean shear rate. The solid red line obtained from the exponential curve fitting using Eq. (17) and optimum values in Table 1, where constants of a , b , and c are a function of shear rate to be determined exponentially decreased. The r^2 value was 0.681.

$$Y = a - b \cdot c^x \quad (17)$$

Table 1: Optimum values for the exponential fitting, Equation (17)

Parameters	<i>a</i>	<i>b</i>	<i>c</i>
Values	5.71	23.46	0.98

It can be seen that the shear rate dependence of the RBC aggregate under pulsatile flow was similar to the one under steady flow. When shear rate is less than 80 s^{-1} for 2 mm/s of velocity amplitude, the number of aggregated RBCs decreased with mean shear rate. In addition, the variation of aggregated RBCs is much higher than that of the other two conditions. However, for 3 or 5 mm/s of velocity amplitude, the reduction of aggregated RBCs as well as the variation of the number of aggregated RBCs was much lower.

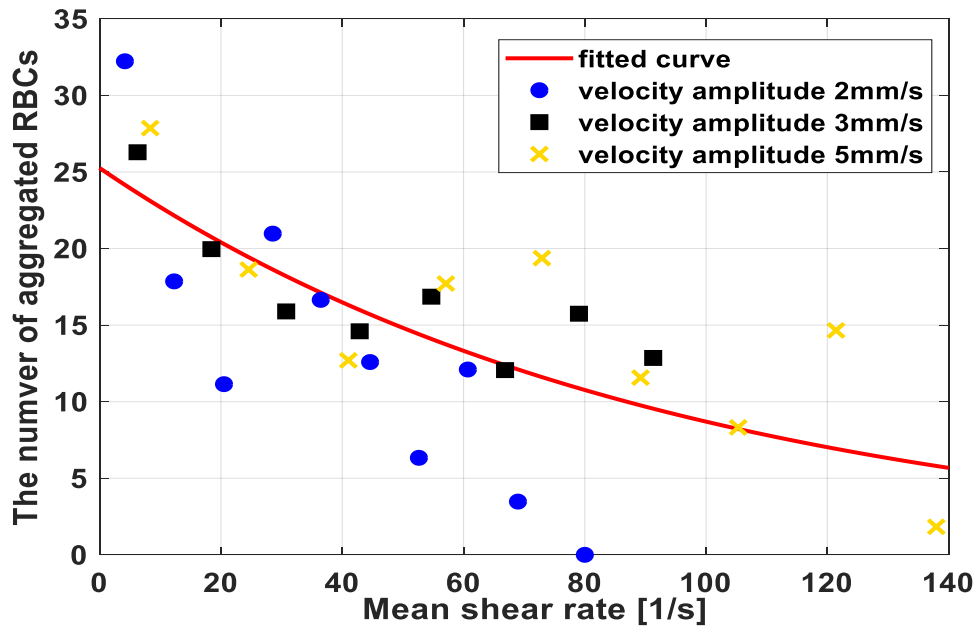


Fig. 11 Relationship between mean shear rate and the number of aggregated RBCs under the steady Poiseuille flow at a hematocrit of 40%. In 2 dimensional rigid tube with 0.1 mm of diameter and 0.3 mm of tube length, the results were obtained by 50 iterations. The symbols of circle (blue), rectangular (black), and cross (yellow) represent the mean values, which are 50 samples derived from the number of aggregated RBCs, with the 2, 3, and 5 mm/s of velocity amplitudes, respectively. The solid line (red) was obtained from the exponential curve fitting with Eq. (12). The optimal constant values are summarized in Table 1 with 0.681 of r^2 .

3.2 Simulation Under Unsteady Flow

3.2.1 Simulation under Womersley flow

In 2D numerical simulation, RBC aggregation was observed under Womersley flow with the rigid and elastic tube wall conditions. The motion of all RBC particles is shown in Fig. 12, which corresponds to the velocity field according to the two tube walls.

The tube wall is arbitrarily designed along x axis and adopted the no slip condition. In our flow model, the amount of flow remains constant and mass flow is neither created nor destroyed. In addition to fluid of the density, volume and shape can all change within the domain with time. Thus, the mass flow rate is derived in Equation (18).

$$\rho_1 A_1 v_1 = \rho_2 A_2 v_2 \quad (18)$$

$$\rho_1 = \rho_2 = \rho \quad (19)$$

Where, A_i and v_i are the flow area and mean velocity of the flow area at the region of i in the tube. ρ_i is fluid density, but the fluid density is constant due to characteristics of incompressible fluid. Therefore, it means that the product ρAV is

recognized as constant mass flow when the area and volume of flow is changed during the time as in the following Equation (20) .

$$A_1 v_1 = A_2 v_2 \quad (20)$$

In this modeling, we implemented the spatial distribution in Womersley flow satisfying the volume conservation with the tube wall expansion and shrinkage as a sinusoidal traveling wave .

$$R(x, t) = A_t \sin(\omega t - k_t x) + B_t \quad (21)$$

The tube radius, which changes in the form of an arbitrary sinusoidal wave with respect to the x direction with time, was expressed as a function of spatial variation of x and temporal variation of t (time step). In Equation (21), A_t determines the degree of tube wall elasticity by the amplitude component of the sinusoidal radial function. B_t is the radius of the tube at mean velocity. (In this case, B_t is 0.05 mm). $k_t (= 2\pi/\lambda)$ is wave number. It is noted that the wavelength (λ) is to satisfy a repeated condition of the flow in the tube. It was designed to increase the velocity at contraction stage, or the velocity decreased in the expansion stage.

Two conditions of the tube are the rigid ($A_t = 0$) and elastic tubes. Fig. 12 (a)

shows the RBC aggregation and disaggregation at the velocity field with the rigid tube wall condition, where velocity changes radially alone. On the other hand, Fig. 12 (b) and (c) represent the simulation results of RBC aggregation with the elastic tube conditions. The difference between the two elastic tubes depends on the degree of elasticity with amplitude (A_t) of radial function. The results are shown in Fig.12 with spatial distribution of velocity field under Womersley flow for different tube elasticity by amplitude of the radial function in Eq. (21). When the wave length ($\lambda = 0.3 \text{ mm}$) and tube radial at mean velocity ($B_t = 0.05 \text{ mm}$) are fixed, the amplitude (A_t) is changed to induce the spatial variation of velocity field. Fig. 12 (b) has high elasticity with $1.5 \text{ }\mu\text{m}$ of amplitude of radial function, which is similar to spatial velocity field in rigid tube. The wall was designed considering the spatial variation of the velocity field as shown in Fig. 12 (c) with amplitude of $3 \text{ }\mu\text{m}$. In the results, there was a difference of the spatial variation of the velocity field of the Womersley flow. As with the RBC kinetics under steady flow, there is no variation along the tube length with random directions of rouleaux. However, when the elasticity of the tube wall increases, the RBC aggregation has the spatial variation along the tube length direction. A parabolic shape of rouleaux was observed in

high elastic tube. As shown in the previous study [31], high aggregate level was observed at low velocity. On the contrary, it was observed that the RBC aggregation decreased as the fluid velocity increased.

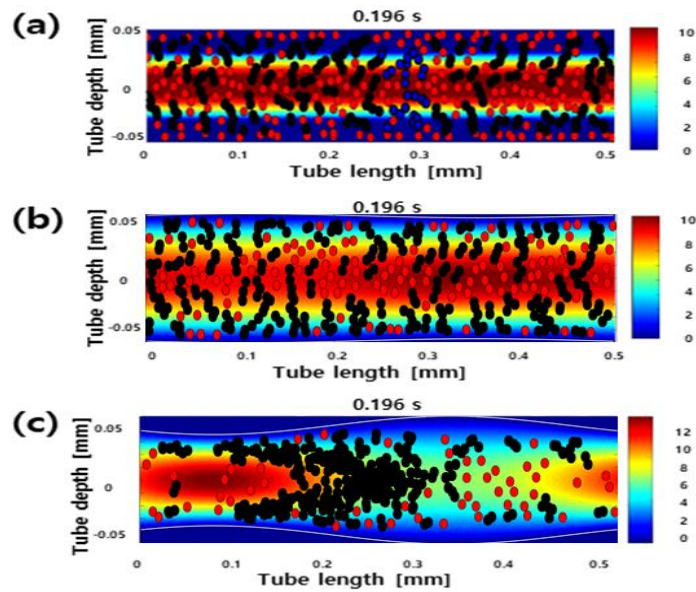


Fig. 12 Snapshots indicate the spatial distribution of the RBCs corresponding to the velocity field under the Womersley flow for the rigid and elastic tube wall conditions. (a) show the distribution of RBCs in the velocity field for the rigid tube ($A_t = 0$). (b) and (c) depict the spatial distribution of the pulsatile flow and the corresponding RBCs with $1.5 \mu\text{m}$ of tube amplitude in radial function and amplitude of $3 \mu\text{m}$, respectively.

3.2.2 Simulation Under Sinusoidal Pulsatile Flow

3.2.2.1 RBC Aggregation Dependent on the Hemodynamic Variation

Fig. 13 shows the formation of RBC aggregates, showing a parabolic shape. At initial time, tRBCs were randomly distributed without overlapping, as shown in Fig. 13 (a). At $t = 0.01$ s, the RBCs began to aggregate and form large rouleaux, as shown in Fig. 13 (b). Then, the rouleaux formed a parabolic shape at $t = 0.05$ s, as shown in Fig. 13 (c). The RBCs and rouleaux located near the center of the tube moved faster than those located near the boundaries. The central rouleaux enlarged and

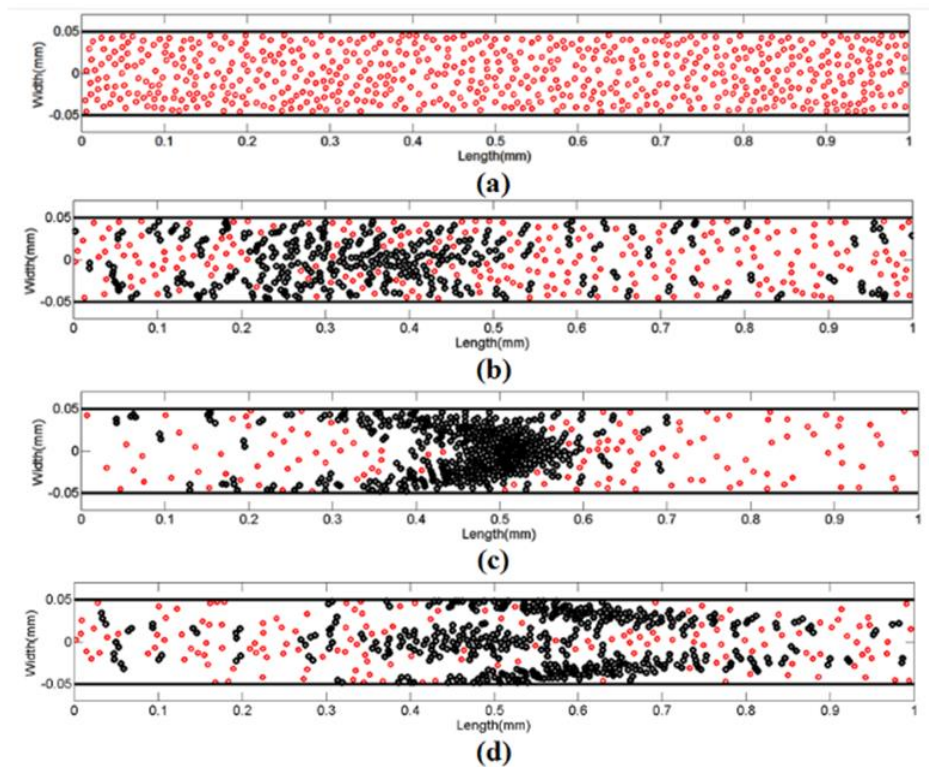


Fig. 13 Four special processes of RBC aggregation under pulsatile flow at 0, 0.01, 0.05, and 0.1 s representing random RBC distribution at the initial time, small rouleaux formation, parabolic shape, and broken parabolic shape, respectively.

the parabolic shape was broken at $t = 0.1$ s, as shown in Fig. 13 (d). Three different velocity amplitudes of 0.5, 1, and 1.5 cm/s with a mean velocity of 2 cm/s and their corresponding MAS are plotted in Fig. 14. MAS increased with time and reached the maximal value at the lowest velocity range and decreased again. The maximal MAS appeared near the lowest velocity range between 0.5 s and 0.7 s under three different amplitudes. As velocity amplitude increased, the peak MAS increased, and mean MAS over a cycle also slightly increased. These behaviors resulted in drastic cyclic variations.

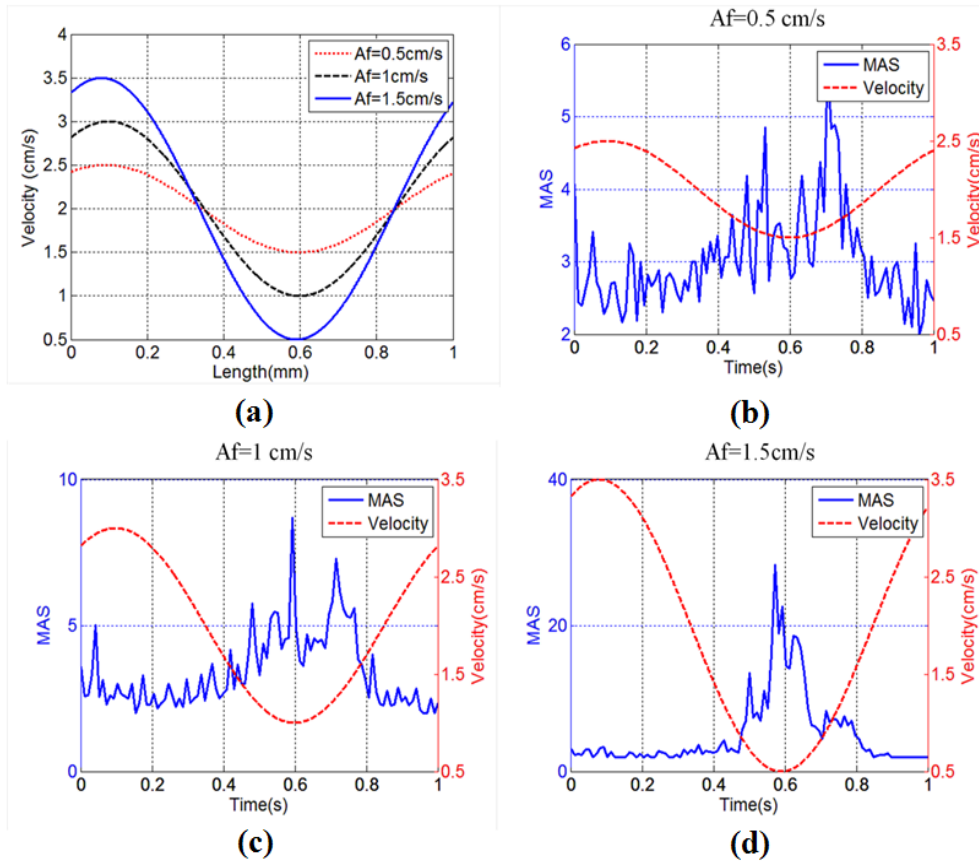


Fig. 14 Comparison of MAS variation under different velocity amplitudes. Fig. 14(a) Three different centerline velocity profiles of the velocity amplitudes of 0.5, 1, and 1.5 cm/s with the mean velocity of 2 cm/s. Fig. 14(b), Fig. 14(c), and Fig. 14(d) represent the MAS that corresponds to three different centerline velocity profiles over one cycle under Poiseuille flow.

The mean flow velocities were changed to 2, 3, and 6 cm/s with the same velocity amplitude of 1.5 cm/s. Fig. 15 (a), and (b), (c), and (d) show the MAS variations with the corresponding mean flow velocity profiles. As mean steady flow velocity increased from 2 cm/s to 6 cm/s, the cyclic variation in MAS weakened and almost disappeared at 6 cm/s. The peak MAS appeared near the lowest velocity range but shifted from 0.9 s to 0.5 s as mean velocity increased from 2 cm/s to 6 cm/s.

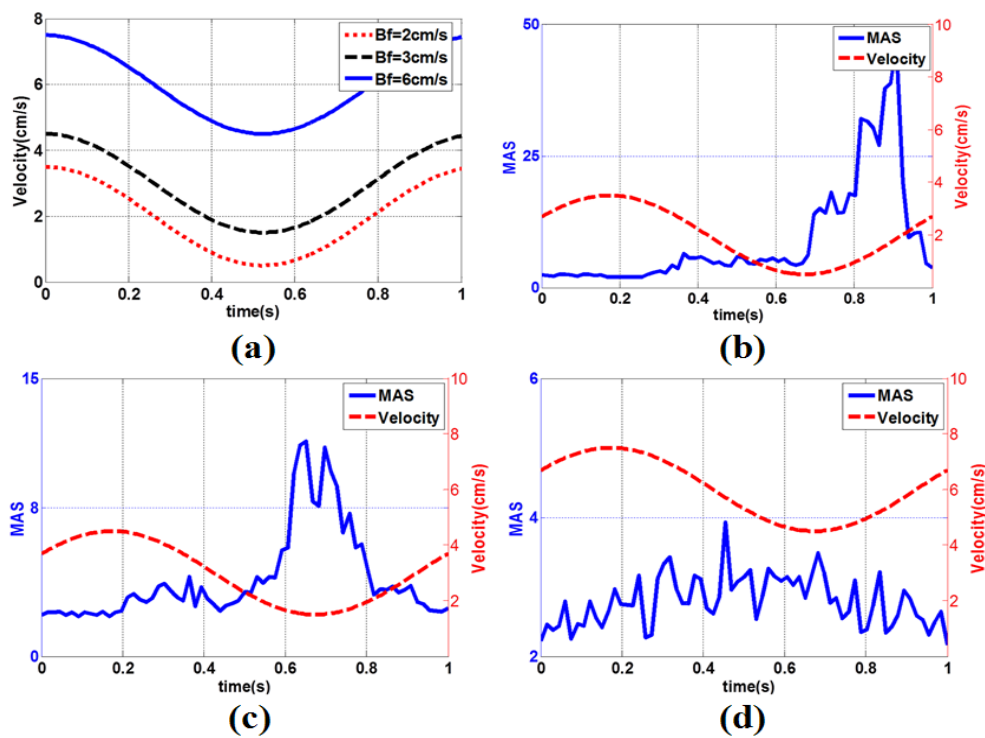


Fig. 15 Comparison of variations in MAS under three different mean flow velocities. Fig. 15(a) Mean velocity was changed from 2 cm/s to 6 cm/s with the same velocity amplitude of 1.5 cm/s. Fig. 15(b), Fig. 15(c), and Fig. 15(d) show MAS variation as a function of time under the mean flow velocities of 2, 3, and 6 cm/s, respectively, and the corresponding velocity profiles.

3.2.2.2 Quantitative evaluation of the RBC aggregation according to the spatial distribution of the fluid field

Table 2 lists the velocity amplitude and the mean flow velocity for the three aggregate levels. Table 2 consists of two cases. In Case 1, the velocity amplitude was fixed at 1mm/s and three mean flow velocities were increased from 3 to 7 mm/s. In the other case, the velocity amplitudes were 0.5, 1 and 1.5 mm/s and mean flow velocities were fixed at 3 mm/s. The three different aggregate levels are illustrated in Fig. 16. The high aggregate condition was an aggregate level in which parabolic shape of the rouleux formation was formed and traveled without breakage over time. In Fig. 16(a), the high aggregate level was computed by using

Table 2: Case1; the fixed velocity amplitude (A_f) and different three mean flow velocity (B_f), and Case 2; the three different velocity amplitude and fixed mean flow velocity under the sinusoidal pulsatile flow

CASE 1

Aggregate level	Velocity amplitude (A_f)	Mean flow velocity (B_f)
High aggregate	1.5 mm/s	3 mm/s
Moderate aggregate	1.5 mm/s	5 mm/s
Low aggregate	1.5 mm/s	7 mm/s

CASE 2

Aggregate level	Velocity amplitude (A_f)	Mean flow velocity (B_f)
High aggregate	1.5 mm/s	3 mm/s
Moderate aggregate	1.0 mm/s	3 mm/s
Low aggregate	0.5 mm/s	3 mm/s

the velocity amplitude and mean flow velocity in Table 2.

At moderate conditions, this formation of the parabolic shape of the aggregated RBC was clearly captured in Fig. 16(b) and broken repeatedly for the flow with 1 mm/s of velocity amplitude and 3 mm/s of the mean flow velocity. It is in good agreement with the previous experimental results [29,33]. In the low aggregate condition, the RBCs hardly formed the formation of parabolic shape with mostly non-aggregated RBCs in Fig. 16(c). In this simulation, the results were evaluated using the number of aggregated RBCs, calculated using the spatial distribution as mentioned in Chapter 2.2.2.

To investigate the RBC aggregation dependence on the shear rate field under sinusoidal pulsatile flow, Fig. 17 shows the number of aggregated RBCs as a function of the mean shear rate over 50 periods for the three different aggregate levels. The mean and standard deviation of each data type are shown as symbols and bars, respectively. It can be observed that the number of aggregated RBCs significantly increased at low shear rate due to RBC aggregation. For the high aggregate level (see the black solid line in Fig. 17), the variation of the aggregated

RBCs was increased. In addition, the aggregated RBCs exponentially decreased when the mean shear rate increased. This tendency is similar for the moderate aggregate level as shown in the red broken line in Fig. 17. However, for the low aggregate condition, the variation of the aggregated RBCs is much less than the other conditions. The results demonstrated that when the degree of the RBC aggregation increased, the variation of the number of aggregated RBCs as a function of the mean shear rate also increased under pulsatile flow. Based on the results, it is also evident that the higher the level of RBC aggregation, the stronger the exponential decrease in the relationship between the RBC aggregation and shear rate.

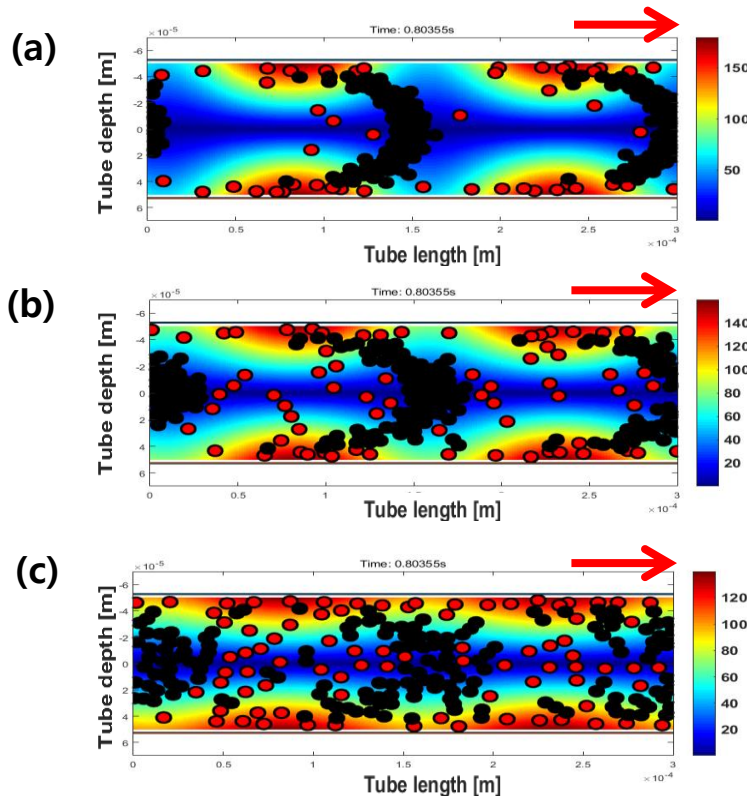


Fig. 16: Three different RBC formation with parabolic shapes under the three different aggregate levels in Case 2. Corresponding flow shear rate field with 238 RBCs (hematocrit 40%) at one time point. The black particles represent RBC aggregation in 2-dimensional rigid tube with 0.1 mm of tube depth and 0.3 mm of tube length. The color bar represents shear rate in 1/s. Fig. 16 (a) High aggregate level conditions promoted the formation of large and ideal RBC aggregation. Fig. 16 (b) At moderate aggregate condition, parabolic and broken-parabolic shaped aggregates was formed periodically. Fig. 16 (c) Low aggregate condition prevented the formation of aggregates, non-aggregated RBCs monodispersed.

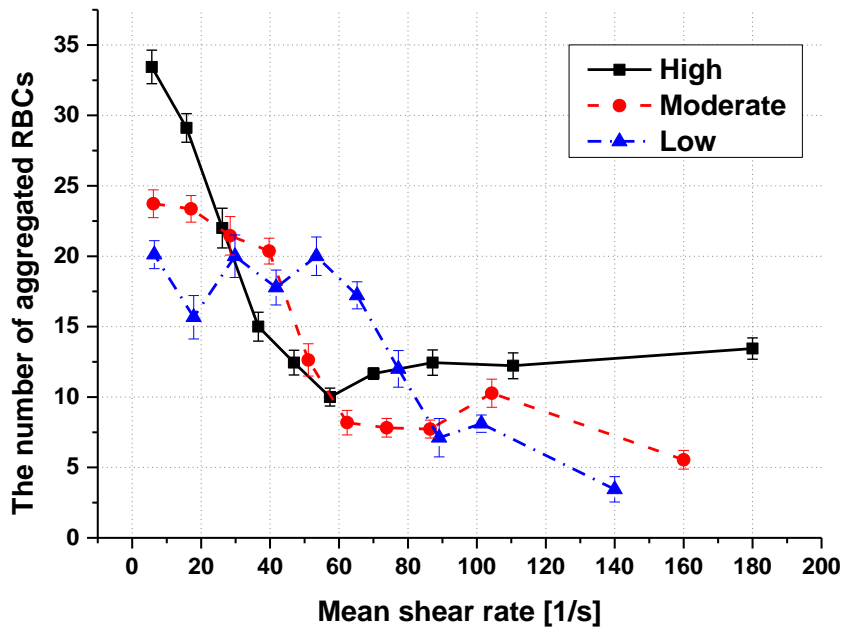


Fig. 17 The number of aggregated RBCs as a function of the mean shear rate for the three-aggregate condition, adapted the three different flow velocity amplitude from 0.5 mm/s to 1.5mm/s with fixed 3 mm/s of flow velocity (From Case 2 in Table 2). The mean (black rectangular, red circle, blue triangular) and standard deviation (black solid line, red dashed line, blue alternated long, and short dash line) are respectively shown as lines and error bar from 50 simulations.

Fig. 18 shows the relationship between the acceleration field and RBC aggregation, which is the temporal gradient of the velocity field with the fluid characteristics of Case 2 in Table 2. All simulation results were repeated 50 times and its average and standard deviation showed the effects of flow acceleration on RBC aggregation. In the simulation under pulsatile flow with the high aggregate condition, the number of aggregated RBCs are, at maximum, approximately 8 mm/s² of flow

acceleration. For the moderate and low aggregate conditions, the maxima are at 6.3 and 3.8 mm/s² of flow acceleration, respectively. The results demonstrated that the maximal aggregation is observed in certain flow acceleration values. Furthermore, when the aggregate level increased, both the peak of number of aggregated RBCs and its variation also increased.

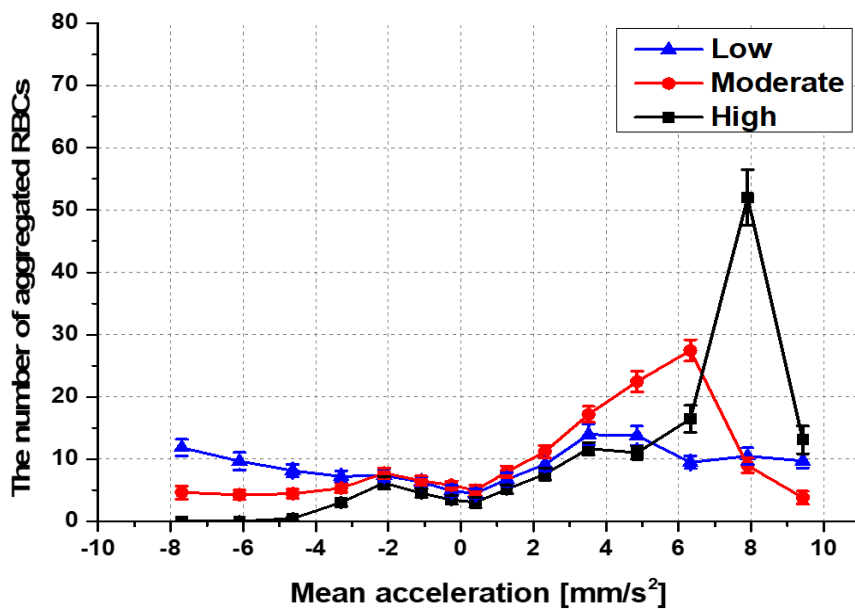


Fig. 18 In the three different aggregate levels, the number of aggregated RBCs as a function of the mean acceleration area under the sinusoidal pulsatile flow. The mean (back rectangular, red circle, blue triangular) and standard deviation (black solid line, red dashed line, blue alternated long and short dash line) are respectively shown as lines and error bar calculated from 50 simulations.

4. Discussion

4.1 Analysis of RBC Aggregation Under Steady Flow

Since shear rate has an important effect on RBC aggregation in a circulatory system [47], many studies have demonstrated that the blood viscosity and shear rate are inversely related under steady flow [6,9,40]. In the Poiseuille flow, the streamlines are horizontal along a straight line. Shear rate is constant in the tube length direction and varies with a constant slope in the radial direction of the tube. Therefore, the shear rate field under the Poiseuille flow is relatively simple, and the number of aggregated RBCs whose variations could be easily estimated. For the range of shear rates of interest, the simulation under Poiseuille flow was performed with several conditions, which are the three different flow amplitudes, to change the maxima of shear rate. Results from the effect of the shear rate on the different flow amplitude are summarized in Fig. 11. As mentioned in the simulation approach, the number of aggregated RBCs in 10 divided areas was calculated, with the same shear rate and normalized area. In the simulation, the 10 divided areas satisfied the conditions that fully contained the single RBC particle with an $8\mu\text{m}$ of diameter in one area. The findings were similar to other experimental results for

the porcine whole blood at 40% hematocrit [48]. The results show the reduction of aggregated RBCs and variation of the number of aggregated RBCs by high mean shear rate.

4.2 Simulation of Womersley flow

In previous studies, we observed RBC aggregation with the forces (interactional forces and hydrodynamic force) under steady flow with radial variation alone. However, the arteries of the human have complex spatial and temporal blood flow fields in the periodic pulsatile flow unlike the veins or capillaries. Therefore, it is necessary to interpret the RBC aggregation with the spatial and temporal variation of the Womersley flow.

In this chapter, we observed the variation of the RBC aggregation with the spatial change of the velocity field along the tube length direction. In addition, we analyzed the distribution of RBC aggregation by temporal and spatial changes under sinusoidal pulsatile flow. Specifically, the degree of RBC aggregation according to the hydrodynamic characteristics, such as amplitude of the velocity and mean flow velocity, was explained and the results of the RBC aggregation

according to the shear rate and acceleration of the fluid were described as a factor affecting RBC aggregation.

4.2.1 Distribution of RBC Dependence on the Tube Wall under Womersley Flow

The purpose of our research is the analysis of interaction of RBC particles by forces of the unsteady flow. For numerical simulation modeling, we adopted the sinusoidal velocity profile obtained by an analytical solution of Navier-Stokes equation in the rectangular tube by S. Tsangaris [42], rather than Womersley flow in a cylindrical tube. We also applied the method described in Fig. 6 to obtain the velocity field in the flow direction (x ; tube length direction).

In this simulation, we observed the RBC motion under Womersley flow with two different spatial variations of the velocity field. First, the simulation was performed without spatial velocity variation in the tube length. The other is the Womersley flow satisfying the volume conservation with traveling wave of elastic vessel wall expansion and shrinkage. RBC motion in the velocity field induced by the two conditions is shown in Fig.12.

The results in Fig. 12(a) shows the motion of the RBCs in a rigid tube without spatial variation of the velocity in the x direction. Each RBC particle was dependent

on the forces induced by the velocity changes in the y direction with time. The '*bright collapsing ring*' phenomenon, which was observed in whole blood measured ultrasound B-mode image under pulsatile flow [28], was not observed from this simulation. Fig. 12(b) and Fig. 12(c) represent the RBC aggregation under Womersley flow in two tubes of different elasticity of the tube. As shown in Fig. 12 (b), the velocity field in the tube with minimal wall motion is similar to spatial distribution of the velocity field under steady flow due to the small variation of the velocity field along the x direction. The simulation results showed small spatial variation which is similar to RBC aggregation under steady flow as shown in Fig. 12(a). On the contrary, the results of the RBC aggregation in Fig. 12(c) showed a high degree of aggregation with the low velocity region and a low degree of RBC aggregation with the high velocity region in the tube. The results are similar to RBC aggregation distribution under sinusoidal pulsatile flow [31] and in agreement with the previous experimental results under pulsatile flow [28]. These results confirmed that the spatial variation of the velocity field affect RBC aggregation. It was found that the forces induced by the flow in the radial direction of the tube formed an RBC aggregation and deformation, and that the variation of the velocity

in the tube length direction increased local distribution of the degree of the RBC aggregation. However, this result requires quantitative analysis in future.

4.3 Simulation Under Sinusoidal Pulsatile Flow

As shown in Fig. 13, particles were located at random positions in the whole tube at a hematocrit of 30%. Under sinusoidal pulsatile flow, RBCs were more likely to form rouleaux at the lower velocity region. Then, the accumulated rouleaux increased in size, and moved faster at the tube center to form a parabolic shape. Then the parabolic shape was broken as a result of faster speed at the central part of the tube. The simulation results are in agreement with the cyclic and radial variation pattern observed from *in vitro* experiments on porcine blood echogenicity [29,33]. The formation and breakdown of a parabolic shape are shown as the bright collapsing ring (BRCR) in cross-sectional B-mode images. Under certain hemodynamic conditions, the BRCR appears as a bright hyperechoic ring that converges from the periphery to the center of the tube and eventually collapses during a pulsatile cycle [29,33]. Meanwhile, longitudinal ultrasound images have been obtained to further describe the processes of RBC aggregation, and a parabolic shape was observed in B-mode longitudinal images [49,50].

Some papers reported the angular dependence of rouleaux under *in vitro* steady and oscillatory flow experiments [29,51,52]. For porcine and equine bloods, an angular dependence was observed at certain specific shear rate conditions, suggesting the cone-shaped aggregated RBCs and orientation at an angle of about 25° with respect to the tube axis [51,52]. Under oscillatory flow, the large rouleaux were formed and aligned at an angle of about 25° near the tube center during flow acceleration from porcine whole blood [17]. This angular dependence may be from partial parabolic shape of rouleaux distribution near the tube center from the simulation results in Fig. 13 (c) and (d). However, ultrasonic investigations of RBC motion at a certain radial position and time and parabolic rouleaux formation are difficult to prove it by the limitations of the physical and measurement conditions of *in vitro* porcine blood experiments. By contrast, numerical simulation enabled the observation of the dynamic processes of RBC aggregation and the formation of a parabolic shape. The simulation facilitated the analytical observation of the formation and breakdown of a parabolic shape. Previous experiments and the present numerical simulation provided similar RBC aggregation trends and parabolic profiles despite their different hemodynamic conditions [31].

4.3.1 RBC Aggregation Dependence on the Hemodynamic Variation

4.3.1.1 Velocity Amplitude

We studied the effects of different hydrodynamic parameters, such as velocity amplitude and mean flow velocity on RBC aggregation under sinusoidal pulsatile flow. As shown in Fig. 14, peak MAS and its mean value increased as velocity amplitude increased. When the velocity amplitude increased, additional rouleaux were formed as a result of the large velocity difference. RBCs were more likely to interact to form large rouleaux in the low velocity region. In the previous experiments, as the peak speed increased from 10 cm/s to 25 cm/s, the BRGR phenomenon became apparent at the high blood flow speed. At a peak speed of 10 cm/s, cyclic and radial variations in echogenicity were minimal. The variation in echogenicity was observed as a BRGR of high contrast at a peak speed of 25 cm/s [33]. In contrast to the simulation results, however, high echogenicity is observed during the systolic phase of the flow. This difference may be attributed to low viscosity, which may cause the phase shift of the peak MAS. Moreover, hysteresis may account for this difference because MAS is a function of shear rate and shear rate history [36]. Finally, the differences in velocity profiles between pulsatile flow

in the previous experiment and sinusoidal pulsatile flow with a mean velocity in the simulation may contribute to this difference. Further systematic studies are required to further understanding of this difference.

Under three different velocity amplitudes of 0.5, 1, and 1.5 cm/s, RBC aggregation was intensified at 0.03, 0.05, and 0.1 s, respectively, as shown in Fig.19. These results indicated that high velocity amplitude results in drastic cyclic and radial variations in RBC aggregation and the formation of a parabolic rouleaux. In porcine blood experiments, temporal variation became apparent as peak speed increases during systole; this behavior coincides with that demonstrated by the simulation results [29,33]. Although the experimental and simulation results cannot be directly compared because of their different conditions (e.g. whole blood viscosity, tube diameter, and velocity profile), the experimental and simulation results presented similar trends.

4.3.1.2 Mean Flow Velocity Dependence on RBC Aggregation

As shown in Fig. 15, the peak MAS decreased as mean velocity increased. As mean flow velocity increased, the mean shear rate increased, consequently reducing rouleaux formation. The smaller variation and peak of MAS with high mean velocity could be attributed to high mean shear rate, as observed in previous *in vitro* experiments. An *in vitro* experiment showed that echogenicity and temporal variation decreased as mean flow increased during flow acceleration [29]. Notably,

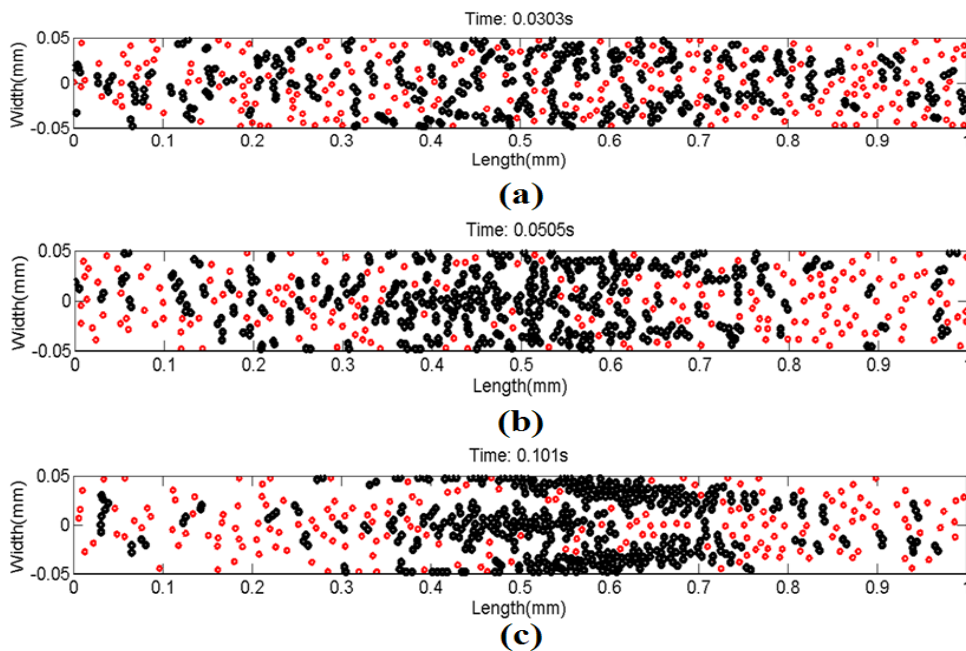


Fig. 19 Three different RBC patterns with broken parabolic shapes under three different velocity amplitudes of 0.5, 1, and 1.5 cm/s and the mean velocity of 2 cm/s.

when we applied pure oscillatory flow in the experiment, the overall echogenicity was weakened as mean steady flow increased from 10 cm/s to 20 cm/s at the

center of the tube. Therefore, the mean shear rate is an important parameter that affects RBC aggregation whether in a pulsatile flow or steady flow system. The simulation results indicated that high mean shear rate should decrease RBC aggregation. Furthermore, the peak MAS shifted to earlier phase from the time of the lowest speed as the mean flow speed increased from 2 cm/s to 6 cm/s. The shift of the peak MAS with peak speed and mean flow speed resulted from the combined effects of shear rate and flow acceleration during a pulsatile cycle. Further systematic studies should be conducted to confirm this result.

4.3.2 Quantitative Evaluation of the RBC Aggregation according to the Spatial Distribution of the Flow Field

The rheological behavior of RBC aggregation depends on the flow conditions, such as amplitude and mean flow velocity. Especially, it is suggested that the RBC formation of parabolic or broken shape under the sinusoidal pulsatile flow is affected by flow conditions [31]. According the flow conditions, we assumed the three different levels of RBC aggregation. Under sinusoidal pulsatile flow in Eq. (12), when the velocity amplitude (A_f) is increased or the mean flow velocity (B_f) is decreased, the aggregate level is high. In contrast, low velocity amplitude or high

mean flow velocity leads to low aggregate level. The hydrodynamic condition is dominant to observe rouleaux, such as parabolic or broken shape. The hydrodynamic factors are summarized in Table 2.

4.3.2.1 RBC Aggregation Dependence on Shear rate

Fig. 17 shows the comparison of the number of aggregated RBCs as a function of the mean shear rate over 5 periods according to three degrees of RBC aggregation under the sinusoidal pulsatile flow with the hydrodynamic parameter of Case 2 in Table 2. The results were obtained at 40% hematocrit (238 particles) in a 2D rigid tube with a tube diameter of 0.1 mm and 0.3 mm of tube length. As shown in Fig. 17, when the mean shear rate was increased, the number of aggregated RBCs was decreased. At the lowest mean shear rate, the average number of aggregated RBCs at the high aggregate level is about 34, moderate condition is about 24 and low aggregate condition is smallest, 20 of aggregated RBCs (see the black rectangular, red circle, blue triangular symbols in Fig. 17). Our simulation results of the spatial distribution of the RBC aggregation according to the shear rate field under pulsatile flow is in partial agreement with previous studies on the inversely relationship between RBC aggregation and shear rate [6-9]. However, the results

are dependent on the variation of amplitude and the mean flow velocity. Fig. 20 shows the three different RBC aggregation and the corresponding shear rate field with the velocity parameters for Case 2. At the higher mean flow velocity with lower velocity amplitude, the RBCs formed lower aggregates under pulsatile flow. In the lower aggregate level, the RBCs did not clearly form a parabolic shape of the rouleaux. Therefore, the relationship between the shear rate and RBC aggregation may not be fully elucidated in this case.

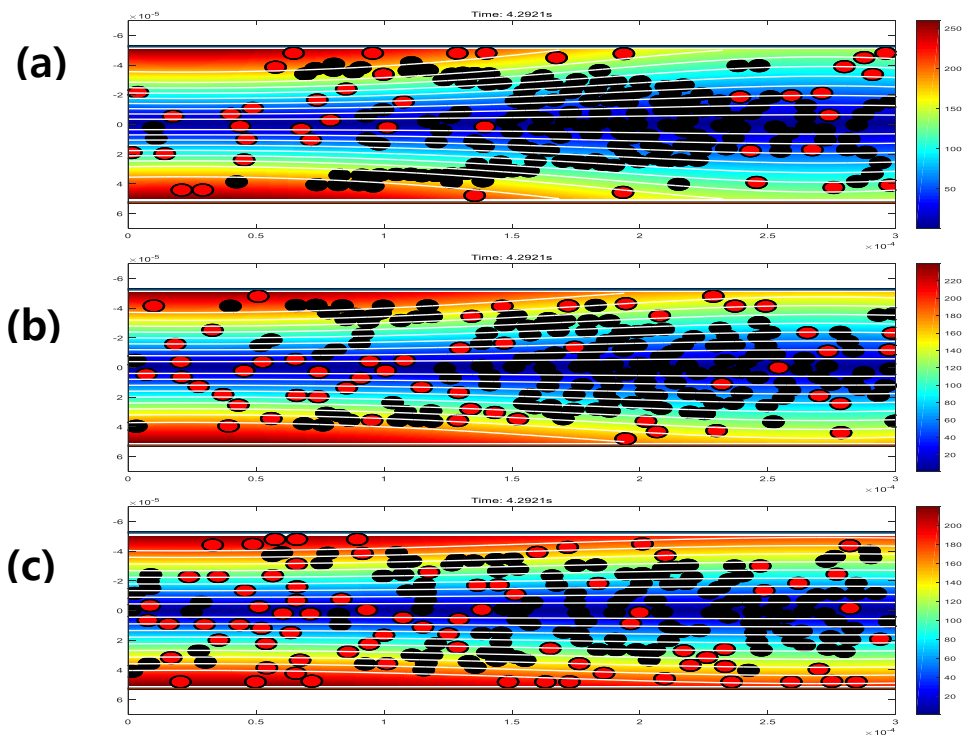


Fig. 20 The snapshots at the same time show the RBC aggregation and corresponding shear rate field for Case 2 in Table 2. Fig. 20(a) is high aggregate level, Fig. 20(b) and Fig. 20(c) show moderate and low aggregate level, respectively.

4.3.2.2 RBC Aggregation Dependence on Flow Acceleration

In the previous experimental studies, a hypothesis for the cyclic and radial variation of echogenicity was suggested as the combined effects of shear rate and flow acceleration under pulsatile flow. The investigation of acceleration influence on RBC aggregation is limited due to the complex spatio-temporal variation under pulsatile flow. In this simulation, we have analyzed the distribution of RBC aggregation as a function of the local mean acceleration. Fig. 18 shows the number of aggregated RBCs as a function of the mean acceleration induced by the velocity field under sinusoidal pulsatile flow. Similarly, RBC aggregation was formed at three aggregate levels with the velocity profile in Case 2 of Table 2. The results present that the highest number, 58, of aggregated RBCs was obtained at 8 mm/s^2 of acceleration in the high aggregate condition. In the moderate and low aggregate conditions, the highest numbers of aggregated RBC are 23 and 12 at the 6.3 mm/s^2 and 3.8 mm/s^2 of acceleration, respectively. The results indicate that high aggregate occurs in a specific acceleration value. The results can be concluded that flow acceleration as well as shear rate is an important factor for RBC aggregation.

5. Limitation and Future Works

5.1 RBC Properties

In this study, the RBC aggregation was considered by the forces based on the elastic and aggregation force with the hydrodynamic force based on the depletion model. Therefore, the interactions of the RBCs and their rouleaux formation were not considered in terms of hematological and biological conditions such as fibrinogen and plasma. We did not consider the cell poor zone. RBCs were assumed as a elastic circular shape in 2 dimensional domain.

5.2 Analysis

Pulsatile flow is difficult to analyze due to the complex spacio-temporal variation. In this study, we divided the shear rate field or the acceleration field of the same value with the same area, in order to quantitatively classify RBC aggregation according to the spatial distribution. The precise scale and criteria for this method are not investigated so that we divided the area into arbitrary number.

In addition, velocity amplitude and mean flow velocity according to the RBC aggregate levels were determined qualitatively by certain conditions. It is required to quantitatively classify RBC aggregate conditions and parabolic shape of rouleaux. In future, the criteria for more precise quantitative evaluation is required through

numerical simulation and experiments and the comparison from the results.

5.3 Relationship between Acceleration and Shear rate

Shear rate of flow as a hemorheological factor affecting RBC aggregation has been known through many experiment and simulation results. However, observation of RBC aggregation under pulsatile flow differs from steady flow. The temporal and spatial distribution characteristics of pulsatile flow are changed by the periodical variation. Therefore, we need to analyze according to the spatial distribution of RBC aggregation under pulsatile flow. In our numerical simulation, the results demonstrated the shear rate as well as acceleration field of pulsatile flow affect RBC aggregation. In future, we will implement the modeling of RBC aggregation to quantitatively analyze the combined function of shear rate and acceleration field of pulsatile flow in order to determine the importance and relationship of the two factors.

6. Conclusions

In this study, we observed the kinetics, detailed processes, and cyclic and radial variation patterns of RBC aggregation under steady and un-steady pulsatile flow. Cyclic and radial variation in RBC aggregation was resulted from interaction forces and hydrodynamic force. We found that the MAS of RBCs and the cyclic variation in RBC aggregation increased with velocity amplitude but decreased with mean flow velocity. Furthermore, we simulated the dynamic process of RBC aggregation in a longitudinal tube to form a parabolic shape. The simulation results for cyclic and radial variation patterns, including the parabolic shape of rouleaux, were in agreement with the previous *in vitro* experimental results obtained with porcine blood [28].

For a quantitative evaluation, we analyzed the relationship between the spatial distribution of RBC aggregation and flow conditions. The relationship between shear rate and RBC aggregation validated the RBC aggregation modeling under the Poiseuille flow. The simulation results were in agreement with the well-known inverse relation between RBC aggregation and shear rate.

We have found that the spatial variation of the velocity field influenced the RBC aggregation from the elastic tube wall condition under the Womersley flow. The spatial variation with the radial and tube length direction by the elasticity of the tube wall is similar to the previous results, the parabolic shape formation at the lower velocity field and its breakdown at the higher velocity field.

In addition, we estimated to analyze of the RBC aggregation under sinusoidal pulsatile flow with shear rate and acceleration fields. The relationship between shear rate and aggregated RBCs is similar to the results under steady flow. In this study, we attempted to explain this phenomenon by RBC aggregation as a function of the acceleration. The results demonstrated that the specific range of acceleration show the maximum aggregated RBCs. With the simple simulation method, the bright collapsing ring phenomenon was observed as shown from the ultrasonic measurement. As a result, we could conclude that acceleration as well as shear rate are important factors under pulsatile flow.

7. References

- [1] G. D. O. Lowe, *Clinical Blood Rheology*. 1988.
- [2] (). *red blood cell morphology*. Available:
<https://theartofmed.wordpress.com/2015/09/05/morphological-abnormalities-of-red-blood-cells/>.
- [3] Y. I. Cho and K. R. Kensey, "Effects of the non-Newtonian viscosity of blood on hemodynamics of diseased arterial flows," *1959 Advances in Bioengineering*, pp. 147-148, 1989.
- [4] O. Baskurt, B. Neu and H. J. Meiselman, *Red Blood Cell Aggregation*. 2011.
- [5] (). *non aggregated Red blood cells*. Available:
<https://www.aiche.org/chenected/2012/11/hitchhikers-guide-drug-delivery-on-location>.
- [6] C. Vlachopoulos, M. O'Rourke and W. W. Nichols, *McDonald's Blood Flow in Arteries: Theoretical, Experimental and Clinical Principles*. 2011.
- [7] D. Paeng, P. Cao and K. K. Shung, "Doppler power variation from porcine blood under steady and pulsatile flow," *Ultrasound Med. Biol.*, vol. 27, (9), pp. 1245-1254, 2001.
- [8] L. Lanotte *et al*, "Red cells' dynamic morphologies govern blood shear thinning under microcirculatory flow conditions," *Proceedings of the National Academy of Sciences*, vol. 113, (47), pp. 13289-13294, 2016.
- [9] R. E. Wells and E. W. Merrill, "Influence of flow properties of blood upon viscosity-hematocrit relationships," *J. Clin. Invest.*, vol. 41, (8), pp. 1591-1598, 1962.
- [10] R. S. Ajmani, "Hypertension and hemorheology," *Clin. Hemorheol. Microcirc.*, vol. 17, (6), pp. 397-420, 1997.

- [11] F. J. Neumann *et al*, "Increased plasma viscosity and erythrocyte aggregation: indicators of an unfavourable clinical outcome in patients with unstable angina pectoris." *Heart*, vol. 66, (6), pp. 425-430, 1991.
- [12] K. R. Kensey, "The mechanistic relationships between hemorheological characteristics and cardiovascular disease," *Curr. Med. Res. Opin.*, vol. 19, (7), pp. 587-596, 2003.
- [13] G. Caimi *et al*, "Haemorheological pattern in young adults with acute myocardial infarction," *Clin. Hemorheol. Microcirc.*, vol. 29, (1), pp. 11-18, 2003.
- [14] R. B. Ami *et al*, "Parameters of red blood cell aggregation as correlates of the inflammatory state," *American Journal of Physiology-Heart and Circulatory Physiology*, vol. 280, (5), pp. H1988, 2001.
- [15] W. Koenig and E. Ernst, "The possible role of hemorheology in atherothrombogenesis," *Atherosclerosis*, vol. 94, (2-3), pp. 93-107, 1992.
- [16] R. Fåhræus, "The suspension stability of the blood," *Physiol. Rev.*, vol. 9, (2), pp. 241-274, 1929.
- [17] G. D. Lowe *et al*, "Relation between extent of coronary artery disease and blood viscosity." *Br. Med. J.*, vol. 280, (6215), pp. 673-674, 1980.
- [18] J. Fuchs *et al*, "Plasma viscosity in ischemic heart disease," *Am. Heart J.*, vol. 108, (3), pp. 435-439, 1984.
- [19] G. Cicco and A. Pirrelli, "Red blood cell (RBC) deformability, RBC aggregability and tissue oxygenation in hypertension," *Clin. Hemorheol. Microcirc.*, vol. 21, (3, 4), pp. 169-177, 1999.
- [20] P. Gyawali *et al*, "Quantitative Measurement of Erythrocyte Aggregation as a Systemic Inflammatory Marker by Ultrasound Imaging: A Systematic Review," *Ultrasound Med. Biol.*, 2018.

- [21] H. Lei *et al*, "Blood flow in small tubes: quantifying the transition to the non-continuum regime," *J. Fluid Mech.*, vol. 722, pp. 214-239, 2013.
- [22] Y. W. Yuan and K. K. Shung, "Ultrasonic backscatter from flowing whole blood. I: Dependence on shear rate and hematocrit," *J. Acoust. Soc. Am.*, vol. 84, (1), pp. 52-58, 1988.
- [23] L. Allard, G. Cloutier and L. Durand, "Effect of the insonification angle on the Doppler backscattered power under red blood cell aggregation conditions," *IEEE Trans. Ultrason. Ferroelectr. Freq. Control*, vol. 43, (2), pp. 211-219, 1996.
- [24] C. Cloutier and K. K. Shung, "Study of red cell aggregation in pulsatile flow from ultrasonic Doppler power measurements," *Biorheology*, vol. 30, (5-6), pp. 443-461, 1993.
- [25] Y. Lin and K. K. Shung, "Ultrasonic backscattering from porcine whole blood of varying hematocrit and shear rate under pulsatile flow," *Ultrasound in Medicine and Biology*, vol. 25, (7), pp. 1151-1158, 1999.
- [26] Y. Chang *et al*, "Study of the effects of flow acceleration on blood aggregation by high frequency duplex ultrasound: Under pulsatile flow," pp. 620-623, 2010.
- [27] P. Cao, D. Paeng and K. K. Shung, "The "black hole" phenomenon in ultrasonic backscattering measurement under pulsatile flow with porcine whole blood in a rigid tube," *Biorheology*, vol. 38, (1), pp. 15-26, 2001.
- [28] D. Paeng, R. Y. Chiao and K. K. Shung, "Echogenicity variations from porcine blood I: The "bright collapsing ring" under pulsatile flow," *Ultrasound Med. Biol.*, vol. 30, (1), pp. 45-55, 2004.
- [29] D. Paeng, R. Y. Chiao and K. K. Shung, "Echogenicity variations from porcine blood II: The "bright ring" under oscillatory flow," *Ultrasound Med. Biol.*, vol. 30, (6), pp. 815-825, 2004.

- [30] D. Paeng, K. Nam and K. K. Shung, "Cyclic and radial variation of the echogenicity of blood in human carotid arteries observed by harmonic imaging," *Ultrasound Med. Biol.*, vol. 36, (7), pp. 1118-1124, 2010.
- [31] C. A. Lee, Q. Kong and D. G. Paeng, "Depletion-model-based numerical simulation of the kinetics of red blood cell aggregation under sinusoidal pulsatile flow." *Biorheology*, vol. 1, pp. 1-13, 2018.
- [32] S. J. Wu and K. K. Shung, "Cyclic variation of Doppler power from whole blood under pulsatile flow," *Ultrasound Med. Biol.*, vol. 22, (7), pp. 883-894, 1996.
- [33] D. Paeng, R. Y. Chiao and K. K. Shung, "Echogenicity variations from porcine blood I: The "bright collapsing ring" under pulsatile flow," *Ultrasound Med. Biol.*, vol. 30, (1), pp. 45-55, 2004.
- [34] S. Chien and K. Jan, "Ultrastructural basis of the mechanism of rouleaux formation," *Microvasc. Res.*, vol. 5, (2), pp. 155-166, 1973.
- [35] S. Chien, "Biophysical behavior of red cells in suspensions," *The Red Blood Cell*, vol. 2, (4), pp. 1031-1133, 1975.
- [36] B. Neu and H. J. Meiselman, "Depletion-mediated red blood cell aggregation in polymer solutions," *Biophys. J.*, vol. 83, (5), pp. 2482-2490, 2002.
- [37] (). *observation of microscop*. Available:
<https://sites.google.com/site/ocmicroreport/live-blood-forms/1-rouleau-rbcs-stacking-or-chaining-together>.
- [38] M. Fenech *et al*, "A particle dynamic model of red blood cell aggregation kinetics," *Ann. Biomed. Eng.*, vol. 37, (11), pp. 2299-2309, 2009.
- [39] Y. Liu *et al*, "Coupling of Navier–Stokes equations with protein molecular dynamics and its application to hemodynamics," *Int. J. Numer. Methods Fluids*, vol. 46, (12), pp. 1237-1252, 2004.

- [40] P. M. Lovalenti and J. F. Brady, "The hydrodynamic force on a rigid particle undergoing arbitrary time-dependent motion at small Reynolds number," *J. Fluid Mech.*, vol. 256, pp. 561-605, 1993.
- [41] Anonymous "definition of Womersley flow," Available: https://en.wikipedia.org/wiki/Pulsatile_flow.
- [42] S. Tsangaris and N. W. Vlachakis, "Exact solution of the Navier-Stokes equations for the fully developed, pulsating flow in a rectangular duct with a constant cross-sectional velocity," *Journal of Fluids Engineering*, vol. 125, (2), pp. 382-385, 2003.
- [43] F. T. Yu *et al*, "Ultrasonic parametric imaging of erythrocyte aggregation using the structure factor size estimator," *Biorheology*, vol. 46, (4), pp. 343-363, 2009.
- [44] J. K. Armstrong *et al*, "Modulation of red blood cell aggregation and blood viscosity by the covalent attachment of Pluronic copolymers," *Biorheology*, vol. 38, (2, 3), pp. 239-247, 2001.
- [45] O. K. Baskurt and H. J. Meiselman, "Cellular determinants of low-shear blood viscosity," *Biorheology*, vol. 34, (3), pp. 235-247, 1997.
- [46] W. Reinke, P. Gaehtgens and P. C. Johnson, "Blood viscosity in small tubes: effect of shear rate, aggregation, and sedimentation," *American Journal of Physiology-Heart and Circulatory Physiology*, vol. 253, (3), pp. H547, 1987.
- [47] O. K. Baskurt and H. J. Meiselman, "Blood rheology and hemodynamics," in *Seminars in Thrombosis and Hemostasis*, 2003, .
- [48] G. Cloutier *et al*, "Power Doppler ultrasound evaluation of the shear rate and shear stress dependences of red blood cell aggregation," *IEEE Transactions on Biomedical Engineering*, vol. 43, (5), pp. 441-450, 1996.
- [49] D. Paeng *et al*, "Three-dimensional reconstruction of the " bright ring" echogenicity from porcine blood upstream in a stenosed tube," *IEEE Trans. Ultrason. Ferroelectr. Freq. Control*, vol. 56, (4), pp. 880-885, 2009.

[50] K. Nam *et al*, "Ultrasonic observation of blood disturbance in a stenosed tube: Effects of flow acceleration and turbulence downstream," *Ultrasound Med. Biol.*, vol. 34, (1), pp. 114-122, 2008.

[51] Z. Qin, L. G. Durand and G. Cloutier, "Kinetics of the "black hole" phenomenon in ultrasound backscattering measurements with red blood cell aggregation," *Ultrasound Med. Biol.*, vol. 24, (2), pp. 245-256, 1998. . DOI: S0301-5629(97)00273-1 [pii].

[52] L. Allard, G. Cloutier and L. Durand, "Effect of the insonification angle on the Doppler backscattered power under red blood cell aggregation conditions," *IEEE Trans. Ultrason. Ferroelectr. Freq. Control*, vol. 43, (2), pp. 211-219, 1996.